Development of theranostic hybrid nanoparticles for phototherapies

by

Ece Çakır

A Dissertation Submitted to the
Graduate School of Sciences and Engineering
in Partial Fulfillment of the Requirements for
the Degree of

Master of Science

in

Materials Science and Engineering

February 8, 2024

This thesis is dedicated to my lovely grandmother, Aynur, who was the most brilliant woman I have ever known.

ABSTRACT

Development of theranostic hybrid nanoparticles for phototherapies

Ece Çakır

Master of Science in Materials Science and Engineering

February 8, 2024

Treatment of bacterial infections, just like cancer is complicated. The effectiveness of traditional treatment methods is often poor. As an alternative, local phototherapies show great promise as a single modality or in combination with traditional therapies. This thesis describes a portfolio of superparamagnetic iron oxide (SPION), quantum dots (QD) and their combination, namely hybrid nanoparticles, as a new theranostic nanoparticle platform to deliver a combination of tracking/imaging and treatment, specifically, photodynamic therapy (PDT) and photothermal therapy (PTT) with enhanced efficiency. Both PTT and PDT and the treatment of cancer and bacterial infections are the targeted applications for such nanoparticles.

A multitude of techniques is employed in the development of such theranostic hybrid nanoparticles considering translation to the clinic. Nanoparticles that can effectively convert light energy into heat are effective in PTT; but for PDT usually photosensitizers, PS, which produces toxic reactive oxygen species (ROS) upon excitation at a particular wavelength, are used. The combination of a PS with a nanoparticle capable of inducing PTT may provide improved therapeutic efficiency. 5-Aminolevulinic acid (ALA), a well-known and FDA-approved prodrug, is used as the, PS in this thesis.

This thesis first describes the synthesis of high-quality SPION and Ag_2S quantum dots, the formation of hybrid structures and the evaluation of their use as theranostics for imaging and enhanced PTT, thereafter. Yet, NIR-emitting and N-acetyl cystein-coated Ag_2S quantum dots emerged as the most promising nanoparticle for imaging & PTT and were applied for the treatment of wound-related biofilm eradication *in vivo*, for the first time in the literature.

This study is partially funded by Scientific and Technological Research Council of Türkiye (TUBITAK, project number: 220S035).

ÖZETÇE

Fototerapiler için hibrit nanoparçacıkların geliştirilmesi

Ece Çakır

Malzeme Bilimi ve Mühendisliği, Yüksek Lisans

Şubat 8, 2024

Bakteri enfeksiyonları kanser gibi oldukça karmaşıktır. Geleneksel tedavi yöntemlerinin etkinliği ise genellikle zayıf kalır. Alternatif olarak lokal fototerapiler tek başına veya geleneksel tedavilerle beraber büyük umut vaat ediyor. Bu tez süperparamanyetik demir oksit (SPION) ve kuantum nokta (QD) kombinasyonundan oluşan hibrit nanopartiküllerin bir portföyünü tanıtır. Tanı ilişkili nanoparçacıklar olarak tanımlayabileceğimiz hibrit nanoparçacıklar izleme/görüntüleme ve tedavi olanağı bulunduran, özellikle fotodinamik terapi, FDT, ve fototermal terapi, FTT, gibi alanlarda üstün bir verim ile çalışan nanoparçacıklardır. Bu parçacıklar için kanser ve bakteri enfeksiyonlarının tedavisi hedeflenen uygulamalardandır.

Kliniğe geçiş düşünüldüğünde, tanı ilişkili hibrit nanoparçacıkların geliştirilmesi için pek çok teknik uygulandı. Işığı ısıya etkili bir biçimde çevirebilen nanoparçacıklar FTT alanında etkilidir. Belirli bir dalga boyunda uyarım yoluyla reaktif oksijen türevleri (ROT) üreten foto-hassaslaştırıcılar, FH, ise FDT için kullanılır. FH ve nanoparçacığın birlikte kullanılması FTT için uygun ortam hazırlayarak geliştirilimiş bir terapötik etki sunar. Bu tezde FDA onaylı ve iyi bilinen bir FH olan 5-Aminolevulinik asit (ALA) kullanıldı.

Bu tez ilk olarak yüksek kalite SPION ve Ag_2S kuantum noktacıklarının sentezini ve hibrit yapıların oluşturulmasını anlatır. Sonrasında ise, bu parçacıkların hem görüntüleme hem de geliştirilmiş FTT kullanımları tanı ilişkili uygulamaları olarak analiz edildi. Böylece, yakın kızıl ötesi ışıma yapan ve N-acetyl cystein kaplı Ag_2S kuantum noktacıklarının, FTT uygulamalarında ve bakteri enfeksiyonlarını yok edebilmesinde kullanılabilecek en gelecek vaat eden parçacıklar olduğu sonucuna varıldı. Yanık ilişkili yara tedavisinde kullanılmak bu parçacık ilk kez kullanılmıştır.

Bu çalışma TÜBİTAK tarafından, 220S035 kodlu proje ile desteklenmiştir.

ACKNOWLEDGEMENTS

First, I would like to express my sincere gratitude to my advisors, Prof. Havva Funda Yağcı Acar and Asst. Prof. Kübra Onbaşlı. I specifically would like to thank Prof. Havva Funda Yağcı Acar for accepting me as a lab member in her lab and for her invaluable input in my scientific life. Asst. Prof. Kübra Onbaşlı made a profound impact on my career expanding my capacity as a grad student, improving my skills in time management and in scientific discussions. I am grateful for all the opportunities that they provided since the beginning of my studies. It was a privilege to be a Funtech member.

I would like to thank Prof. Füsun Can, Prof. Duygu Avcı Semiz, Assoc. Professor Uğur Ünal and for being on my thesis committee and for their valuable contributions. Especially, Assoc. Prof. Uğur Ünal was always there for me when I needed help, guidance, and assistance. It was really capacity developing for me to join experiments with him. My journey could not really link to Prof. Duygu Avcı Semiz since she did not give lectures during my bachelor when she was intended to do. Her Polymer Chemistry Laboratory lesson was long-awaited. Then, I went to her lab many times both to chat with my closest friends but also to conduct experiments. She was always caring and welcoming. Prof. Füsun Can did not just participate in my thesis committee but she was also one of the collaborators that we proceeded this study with. Together with her team, she was always helpful in frutiful discussions about data and experimental setup. If she did not explain it to me, I would not be able to learn about bacteria and infections.

I would especially like to thank Prof. Alphan Sennaroğlu for sharing his expertise in laser set-ups and for giving his invaluable suggestions over my data. My scientific discussions with him led me to carefully examine laser calculations and modify them accordingly. From Laser Research Laboratory ran by Prof. Alphan Sennaroğlu, Dr. Yağız Morova was always there both during laser and *in vivo* experiments. His kindness and eagerness to teach motivated me even in challenging times. I feel that I am lucky enough to have worked with him in many different experiments. Also, from Prof. Füsun Can's research group, Dr. Nazlı Ataç worked as our collaborator in bacteria and biofilm studies. She conducted bacteria and biofilm experiments in Koç University Hospital. She is extremely helpful not only when concerning the experiments but also in commenting on the data. We helped each other a lot both during our visits back and forth to the hospital, and in animal experiments at Koç University Research Center for Translational Medicine (KUTTAM) Animal Research Laboratory.

I would like to express my appreciation to Dr. Barış Yağcı who supported me with fruitful discussions and helped me a lot with my characterization procedures at KUYTAM. My time with him was always funny, humorous, but educative. My heartfelt gratitude goes to Dr. Hadi Jahangiri at KUYTAM, who was always accessible and supportive of me when I needed assistance or direction. He taught me a lot and was always there to guide me whenever I needed it.

There is a new Funtech member whom I know beforehand: Türkan Gençoğlu. Dr. Türkan Gençoğlu used to give lectures to us during my undergrad days as our TA, but now, I'm glad to have called her as a colleague. She was always helpful and ready to convey her experience.

I am grateful for the friendships that I had in Funtech, especially with Ahmet Ferid Fırat, Mine Demir, Dilara Sipahioğlu, and İrem Acar. Their support, encouragement, and friendship in and outside of the experiments were valuable. Especially, I am glad that I can call Ferid as my collaborator for a nanoparticle that we are extremely happy about. Also, Ali Arı, our undergraduate student from the Faculty of Medicine was my first undergraduate student who I hopefully managed to teach my experimental procedures and successfully conveyed the best of my knowledge. His presence truly challenged me and opened a new horizon on my way to improve my communicational skills at an academic level. I would like to express my appreciation to one of my close friends, Elif Öykü Alagöz. She was the source of laughter even in the most challenging times. I would like to thank Emir Ardalı for being a great friend and for his help especially in Origin. It is always good to have him in my personal and academic life since he is extremely kind and helpful.

I would like to express my gratitude to my beloved family, especially my grandparents Hava and Hüseyin Çetinkaya for their endless support, joy, and love. It was a joyous ride to be alongside my family against all difficulties. My father, Eray, and my mother, Sibel, together with my brother Cem Çakır were always there for me no matter what. There was also one person who put his unconditional support even though struggled a lot on the way, Deniz, whom I love truly as my dear friend even though we have been distant.

I would like to acknowledge the Scientific and Technological Research Council of Türkiye (TUBITAK, project number: 220S035) for financially supporting this project. I am also thankful fort he scholarship given by TUBITAK-BIDEB 2210/A.

Table of Contents

List of Tables

List of Figures

Abbreviations

3MPA	3-mercaptopropionic
APR	Acute-phase response
ATPMS	(3-Aminopropyl)triethoxysilane
CFU	Colony Forming Unit
Da	Dalton
DI	deionized
DLS	Dynamic Light Scattering
DMEM	Dulbecco's modifed Eagles medium
DMSO	Dimethyl sulfoxide
EtOH	Ethanol
FBS	Fetal Bovine Serum
FTIR	Fourier Transform Infrared Spectra
LA	Lauric Acid
MW	Molecular weight
MTT	Thiazolyl blue tetrazolium bromide
Na_2S	Sodium sulfide
$Na_2S_2O_3$	Sodium thiosulfate
NIR	Near-infrared
PAA	Poly(acrylic acid)
PBS	Phosphate buffered saline
PDT	Photodynamic Therapy
PEG	Polyethylene glycol
PS	Photosensitizer
PTT	Photothermal therapy
RT	Room temperature
SD	Standard deviation
-SH	Thiol
TEM	Transmission electron spectroscopy
TUBITAK	Scientific and Technological Research Council of Turkey
TGA	Thermal gravimetric analysis
UV	Ultra violet

XPS	X-ray photoelecton spectroscopy
XRD	X-ray diffraction

Chapter 1: Introduction

Smart materials are on the cutting edge of research either with improved functionalities or novel properties. These materials can be at the heart of many applications varying from biomedical purposes to green energy solutions. Mimicking the nature mostly, endeavouring to comprehend how nano and electronic systems work in harmony, nanoscience becomes handy. Recent advances for engineering innovative improvements and developing smart composites need nanoscale reorganization.

Norio Taniguchi coined the word "nanotechnology" for the first time in history in 1974. Later, Feynmann transformed a broad understanding of nanoscience. This approach makes the process simpler to launch fresh new nanomaterials tactics and smart material technologies.[1] Especially, noble metal nanoparticles gain prominence due to their unique features, adaptability of novel technologies compared to bulk metals. Nanoparticles with abilities to respond to environmental changes while maintaining normal functions are promising agents to modify their characteristic properties such as structure, surface area, size, permeability, and such.[2], [3]

Conducting the nanoscale reorganization, engineering such materials often need hybridization of different materials. These nanoparticles have many different versions due to their strong adaptability. Unlike conventional materials, these nanoparticles are highly stable, flexible and can be altered for different occasions and usage. Among such nanoparticles with a variety of functions, semiconductor quantum dots (QDs) and superparamagnetic iron oxides (SPIONs) draw attention at the highest degree.

The fusion of these two materials produces hybrid nanoparticles with both of their properties present and extended to a considerably more advanced structure. Hybrid nanoparticles draw attention since they can be much more efficient at the nanoscale.

1.1 Magnetic Phenomena

The magnetic field is a crucial factor to consider when manipulating nanoparticles. Iron, a magnetic material, and functional materials like coatings can be used to construct

magnetic nanoparticles.[4] Living complexes and bio-applicable materials can also contain magnetic materials. Therefore, it is important to mimic these particles as they are already used in natural substances and can be applied in areas such as biosciences and biotechnology. Magnetic materials can be used in various functions, including biomedicine, tissue-specific targeting, magnetically responsive colloidal crystals, microfluids, and magnetic resonance imaging.[5]

Magnetic properties can depend on many characteristics including morphology, microstructure, phase composition, also interfacial functionalities. There is a strong correlation between magnetic properties and size of a nanoparticle. Particle size can decrease via decreasing the Fe layer thickness. In a study, Carbucicchio suggested that superparamagnetic response can increase as Fe layer thickness decreases whereas ferromagnetic percentage can decrease respectively.[6]

1.1.1 Superparamagnetic Iron Oxide Nanoparticles

As one of the most crucial elements that changed history, iron still is an essential material. The long history of iron dates to 3500 BC in Egypt, and it is still profoundly utilized in many areas and applications thanks to its ease of manufacture.[7] Not only crucial to manufacture systems, iron is mired in biochemistry thanks to iron metabolism mostly developed by cellular iron.[8]

As iron readily forms iron oxide, it is evident that iron oxide also has its way back to prehistoric times. Iron oxide-rich mineral clay was one of the first paints used in human history. Even through the Renaissance or Impressionist paintings, iron oxide can be seen. Nowadays, the widespread use of iron oxide in geochemistry, weathering, and corrosion science is owing to its outstanding technical properties. Iron oxide demonstrates outstanding chemical properties in biomedicine, the development of magnetic devices, heterogeneous catalysis, and photocatalysis. Iron readily forms iron oxide and this is its mostly found form.[9], [10] Iron oxide nanoparticles (NPs) can be found in a variety of applications, including magnetic resonance imaging (MRI), hyperthermia, and drug delivery.[11]

There are many different iron oxide phases that can be found in a nanoparticle. One of the most stable phases is hematite (α- Fe_2O_3). Depending on their size, different phases, in this case it is magnetite (Fe_3O_4), in an iron oxide nanoparticle (IONP) has the ability to demonstrate superparamagnetic behaviour.

Superparamagnetism is generally found in the magnetite domain, however superparamagnetic iron oxides (SPIONs) can have various magnetic domains, such as maghemite, Fe_2O_3. Out of 8 domains generally present in a magnetic nanoparticle, maghemite, hematite and magnetite represent generally superparamagnetic nanoparticles with critical functionalities such as magnetic, catalytic, and biochemical properties.[12], [13] Superparamagnetism readily links to the behaviour of materials under magnetic fluctuation and ease of magnetization. Magnetic anisotropic energy is much larger than thermal energy in bulk iron, however, thermal energy in a nanoparticle can sufficiently invert magnetic spin direction. The blocking temperature is lower with smaller nanoparticles. As a result, magnetisation is easily flipped.[14] In contrast to bulk samples, features of superparamagnetic particles differentiate at the nanoscale level so behaviours of these particles are specialized to their nano size. Crystalline and bulk samples tend to possess various magnetic ordering where crystalline ones have stronger magnetic ordering. Additive contribution to entropy must be present due to magnetic moment disorientation in the SPIONs. Any input to entropy is directly related to Curie Temperature, a threshold below which particles express a superparamagnetic response. Increment in size refers to less dependence of the disorientation on T_c. [15] In the magnetic field, if there is a single orbiting electron, it can decide response of a material. Plotting the magnetic induction B, can also be exemplified as flux density per square meter, at where magnetic field, H, is applied. When magnetization is against H, permeability of free space effect is involved. Vector field density of induced magnetic dipole moments, which are derived via electric charge movement or acceleration towards a direction, may be plotted via formula $B=\mu 0(H+M)$. This connection addresses a prominent information due to magnetization that can be derived from M versus H loop. Equation of H maintains separation by an energy barrier of height. Energy difference is equal to KV where K refers to unaxial anisotropy constant compassing both the magnetocrystalline and demagnetizing additions and V points out the volume of the nanoparticle.[16] Magnetic anisotropy emphasizes a dependence on the internal energy towards a spontaneous magnetization direction. So that, nanoparticle having a magnetic component easily has a magnetic anisotropy.[17] If KV is higher than k_BT, nanoparticle magnetic moment cannot be switched automatically where the system tends to behave like a permanent ferromagnet. Magnetic anisotropy putting less effect, thus KV being smaller than k_BT, spontaneous switches within dipoles can be demonstrated. So, superparamagnetic nanoparticles arise thanks to this spontaneity.[16]

1.1.2 Synthesis Method for Different SPIONs

SPIONs can be synthesized via different routes. Generally, a nanomaterial may be produced via a top-down or bottom-up synthesis approaches. The top-down technique entails breaking down a bulk material into nanosized particles. Some bottom-up preparation methods of SPIONs include sol-gel, electrodeposition, and colloidal precipitation.

Co-precipitation of iron salts in an aqueous medium is environmentally friendly and low cost. Reaction time needs to be carefully addressed. Otherwise, oxidizing agents might be overly expressed and lead to Fe^{+3} creation more than necessary. If Fe^{+3} is much more obtained, a weak magnetic response may be generated.[18] In Szalai's procedure, ferrous and ferric chloride are utilised together for coprecipitation of black magnetite nanoparticles triggered by the addition of NaOH at moderate temperatures. [19]

$$FeCl_2 + 2{\cdot}FeCl_3 + 8{\cdot}NaOH = Fe_3O_4 \downarrow + 8\,Na^+ + 8\,Cl^- + 4{\cdot}H_2O$$

Figure 1.1: Synthesis of iron oxide

All superparamagnetic iron oxide nanoparticles in our group are synthesized via co-precipitation method of both ferric and ferrous chloride. Addition of coating materials provided formation of colloidal magnetite nanoparticles, NPs. Colloidal stability gained is preserved for very long time.

SPION can be synthesized with many different coatings to fulfil different needs, including stability, control of aggregation and surface characteristics. Strong interaction of the coating with the iron oxide crystal ensures long term chemical and colloidal stability. Small crystal size and large surface area of nanocrystals brings in new challenges such as susceptibility of these nanoparticles to oxidation and congestion. That is why coating is vital as a protective layer. [20] Coating also is a key to challenge particle agglomeration and colloidal dispersion.

1.1.3 SPIONs with different coating materials

SPIONs can have many different coatings based on desired applications. Surface charge originating from the coating is an important parameter to be decided when degradation, *in vitro* and *in vivo* applications are considered. [21] Furthermore, changes in the pH of the environment can modify a particle's surface charge, and even its

hydrodynamic size because measurement of hydrodynamic size is ultimately tied to preserving ions at the environment. Charged nanoparticle surface is shown to suppress agglomeration and stabilise dispersions.[22]

Our group is specialized in stabilizing SPIONs with different coatings including polyethylene glycol, PEG, (3-Aminopropyl) trimethoxysilane, APTMS, Polyacrylic acid, PAA and Lauric acid, LA. All these coatings can be utilized for different purposes. PEG coating may provide biocompatibility and neutral surface charge in addition to small hydrodynamic size which are effective parameters to extend blood circulation time. [23] PAA coating is shown to provide extensive stability via negative surface charge and strong adsorption to iron oxide surface with multidentate attachment. Also, PAA coated SPION was proven non-toxic in the *in vivo* experiments. SPIONs coated with LA or oleic acid are well-known in the literature which produces hydrophobic SPIONs, providing organic colloidal ferrofluids. SPIONs synthesized with excess LA in water constitutes a LA bilayer coating. LA monolayer-coated iron oxide nanoparticle can be transferred into chloroform or toluene as shown by Yağcı Acar et al.[24]

Silane-based coatings for SPIONs are also in use. APTMS, as a common alkoxysilane used for SPION coating, produced an amine functionalised surface. APTMS is used for covalent attachment of silane to the iron oxide and not prone to desorption.[25] SPIONs with APTMS coating may easily be produced in aqueous environment to produce cationic, colloidal, aqueous SPIONs. [26]

1.1.4 Biomedical Applications of SPIONs

SPIONs, a wide combination of magnetite and maghemite, have unique magnetic properties, preferable chemical stability, and low toxicity especially when compared to other magnetic materials such as nanoparticles including Co, Mn, and Ni. SPIONs received a lot of attention lately in plenty of biomedical applications such as magnetic resonance imaging, gene delivery, tissue engineering, magnetic targeting-based sorting. Moreover, these materials have been preferred as therapeutic and theranostic agents especially in cancer treatment due to its magnetic hyperthermia and photothermal potentials. [27]

One of the most established biomedical applications of SPIONs is the generation of contrast in magnetic resonance imaging, MRI. Stronger magnetization of SPIONs compared to paramagnetic or ferromagnetic materials in an applied magnetic field results in stronger contrast in a tissue. Lack of a net permanent magnetization in the absence of

a magnetic field is critical for its safety and advantages reducing the likelihood of agglomerated particles.[28]

Other medicinal uses consist of radionuclide treatment, photothermal therapy, thermal immunotherapy, and a boost of thermo and chemotherapy.[29] In our group, PTT effect of many different SPIONs was studied. APTMS coated SPION, and an organic photosensitizer, indocyanine green (ICG), loaded APTMS-SPION were investigated *in vitro* PTT study. It was found out that NPs carrying 18–275 μg Fe/ml caused a mild hyperthermia. PTT effect of free ICG was also studied, however, it did not achieve an outstanding result. The viability of MCF7 cells dropped to 22% with the highest ICG concentration. In the same cell line with the treatment of ICG loaded APTMS-SPION there was almost a complete killing even with lower concentrations of ICG.[26] This enhanced treatment was shown in Figure 1.2.

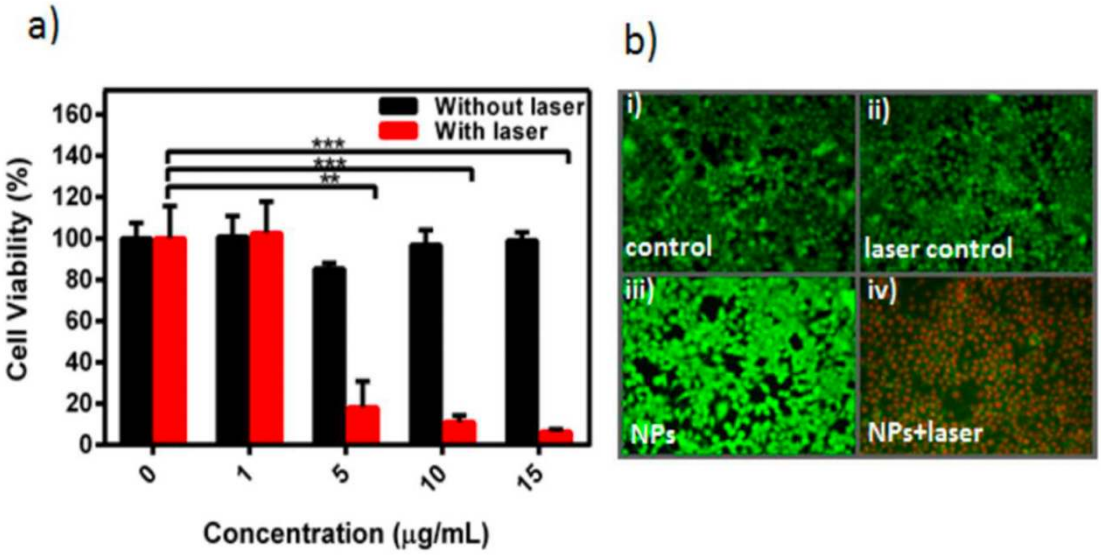

Figure 1.2: Cell viability of MCF7 cells and MCF7 cells stained with live/dead assay kit

Our group is also keen on investigating antibacterial effects of SPIONs. ICG loaded SPION, free ICG, APTMS-SPION were tested over 4 different bacteria and biofilm eradication was performed with an exceptionally high log reduction of 6,5 in *K. pneumoniae* type. As explained within Figure 1.3., compared to other data groups ICG loaded APTMS-SPION performed the best biofilm eradication functionality with 808 nm laser irradation applied 1150 mW.

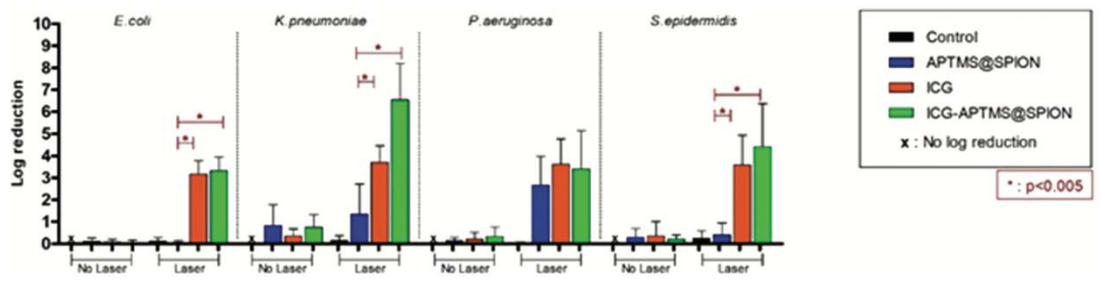

Figure 1.3: Antibacterial effect of SPIONs in biofilm eradication within a span of different bacteria

1.2 Photoluminescence

1.2.1 Quantum Dots

Quantum dots are crystalline semiconductor nanoparticles with infinitely tiny sizes, thus require a name as "dot". These nanoparticles define quantum confinement effect in three dimensions even though the name does not accentuate a dimension.

A wide range of size dependent unique traits, such as size dependent optical properties, namely absorption and luminescence put QDs in the radar of many different applications. QDs demonstrate size dependent and strong luminescence as well as better photostability compared to organic fluorescent dyes. These make QDs as valuable alternatives to organic fluorophores in biomedical imaging.[30]

One of the first methodologies designed in QD fabrication involves toxic precursors and high temperature synthesis in organic solvent producing hydophobic QDs that require post-synthetic procedures to transfer them to aqueous solutions and render them biocompatible.

Describing the significance of QDs, first QD ever known to history is a PbS QD that is initially discovered approximately 2000 years ago. Later on, blue shift in the optical spectra with a help of CuCl silicate glass in nanosize is observed. That observation is followed by a declaration of hypothesis from Efros suggesting that either size or stoichometry of CdS_xSe_{1-x} can effectively influence a differentiation in the colour of glass.[31] Since then, discussion of quantum size effects has been drawing a lot of attention. As a milestone in history of quantum dots, 2023 is an eccentric and a highly special year since QDs are accknowledged with a Nobel Prize.

Notably, in 1985 Ekimov and Efros expressed the significance of quantum size effect in semiconductor QDs, which they used to call as “microcrystals” those days, as shown in Figure 1.4. [32] They announced a new type of material that is capable of

demonstrating quantum size effects in accordance with its size, spectroscopic shift and the fundamental absorption edge. Provided that, as size of these micro crystals, later to be renowned as quantum dots, decreases, a major short wavelength shift of the exciton lines is observed.

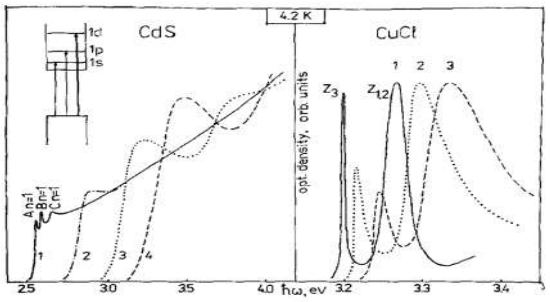

Fig.3. Size dependence of the absorption spectra of CdS and CuCl micro-crystals.
CdS:(1) - $\bar{a}$ =320 Å;
(2) - $\bar{a}$ =23 Å;
(3) - $\bar{a}$ =15 Å;
(4) - $\bar{a}$ =12 Å;
CuCl:(1) - $\bar{a}$ =310 Å;
(2) - $\bar{a}$ =29 Å;
(3) - $\bar{a}$ =20 Å.

Figure 1.4: Size dependence of the absorption spectra of CdS and CuCl microcrystals

In the figure, the comparable relation between the size and the wavelength shift of the absorption edge is established. Similarity of exciton radius and the QD size highlights the loss of exciton structure in the material.

1.2.2 Quantum Confinement

In 1970s, a terminology as quantum confinement was coined to the literature when Molecular Beam Epitaxy (MBE) is utilised in production of thin layers from a variety of different materials with atomic precision thickness.[33] Quantum mechanics is taught to be observed inside a tiny area of a substance where it influences the size and energy relationship of a nano system. For instance, a material can be transparent at a photon energy, but its bulk form may absorb strongly. Moreover, atomic layer thicknesses can be used in tuning band edge. A material's band edge can be blue shifted when exposed to the correct amount of confinement energies. Therefore, when tuning the strip edge of a material, its size, which can also be interpreted as thickness, is of great importance.

The recombination of a hole in the valence band and an electron in the conduction band is another example of spatial confinement. Due to the elimination of free electrons and the stabilization of holes, the concept of recombination maintains an equilibrium in steady state. There are two main clusters of recombination, radiative and non-radiative.

When an electron moves from the conduction band to the valence band during electron-hole recombination, a photon is released.[34] Three optical phases of photon emission can be distinguished as spontaneous, absorption or gain emission, and stimulated emission. Non-radiative recombination may also occur in three different modalities. Auger recombination establishes if the certain amount of energy released during electron-hole recombination promotes to another electron to excite in the same band to higher energy levels. This radiation generates an excited electron maintaining a thermal equilibrium via depleting its energy to lattice vibrations. Another kind of non-radiative recombination originates through defects, wherein electrons recombine with holes via defect energy in the bandgap.

These defects are evolved in many semiconductors either intentionally or unintentionally. Electrons can get trapped by an energy state inside the defects which can only be recombined with a hole only if it also attains same energy. Lastly, recombination can be occurring through dangling bonds on a surface which act as exposed surfaces to absorb impurities. Expanding to a localized centre of defects, exposed surfaces can be utilised to recombine an electron which also bolsters a preferred enhancement for injection lasers.

In quantum dot scale, an exceptionally important factor would be nanocrsyalline nature of these materials. Depending on the size and shape of the quantum dots, electronic and optical properties alter. Nanomaterial exhibits these functions in a range starting from an individual molecule to bulk semiconductors. Quantum dots are nanocrystalline semiconductors produced either by single elements such as Ag, Si, Ge or compounds such as CdSe, CdS. [35] These semiconductors are defined in separate groups according to their band gap differences. Type of band gaps is also critical when QDs are considered. The band gap introduces minimum amount of energy for an electron to be excite from its bound state. Energy difference of an electron between its free and bound state refers to its band gap. The place left empty when an electron is excited is called a hole, so called a positively charged particle on the crystal structure. [36] Defined as carriers, both the electron and the hole attend conduction.

Crystal size of a nanoparticle generally introduces a quantum confinement state in which atoms demonstrate enhanced properties. Strong quantum confinement is exhibited when the size of a nanoparticle is extremely small, smaller than the Bohr radius. According to Ekimov, for example, CuBr and CdS may have Bohr exciton radius 1,8 and 2,8 nm respectively referring to intermediate confinement.[37] It indicates that the

quantum dot radius is narrower than the Bohr radius of either carrier but not both. In a case of quantum dot radius exceeding the Bohr radius of both carriers, excitons encounter weak quantum confinement. As it is demonstrated in Figure 1.5, Bohr radius should at most be equal to radius of QD to have strong quantum confinement effects. Thus, it can be stated that the crystal size strongly correlates with confinement effect.

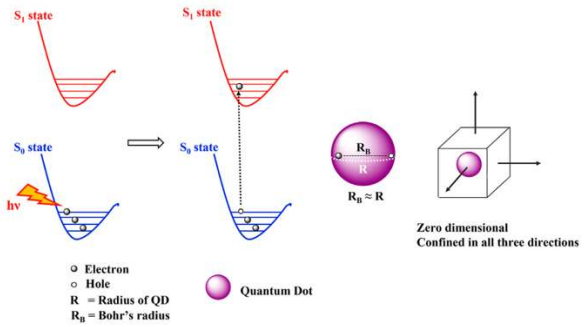

Figure 1.5: Quantum confinement effects seen in QDs *[38]*

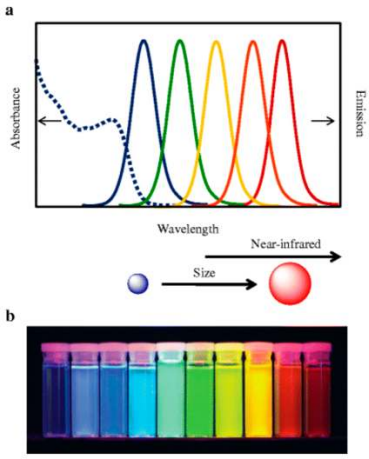

Figure 1.6: Size tunable emission spectra of QDs

The Bohr radius is distinctive for each semiconductor so that quantum confinement effects are studied at smaller dimensions compared to the Bohr radius. A quantum dot is only constituting of a few atoms and when it is excited via photon, the valence band of the electrons form the excitons. The size of an exciton becomes similar to the size of the QD resulting in rigid atomic like energy levels as well as the spatial exciton confinement.

Behaviours of this exciton such as being excited and relaxing back to the lower energy state results in several actions. Thanks to its movement, QDs can emit some energy and can be involved in processes like fluorescence.[38] Emitted energy can be established as the total of bandgap energy, quantum confinement energy as well as the exciton energy. Therefore, small size in QDs refers to large band gaps so that more energy

would be necessary to form the exciton. Similarly, more energy will readily be emitted during luminescence process. This causes a size dependent tunable emission property of the QDs as it can be followed in Figure 1.6. [39]

1.2.3 Near Infra-Red Emitting Quantum Dots

Tunable optical properties can serve as an option to emit energy over a broad selection of wavelength. Biomedical approaches indeed require near infrafred (NIR) emitting QDs. QDs emitting in the visible region usually requires excitation in ultra-violet, UV, region which damages the healthy tissue due to its high energy. Additionally, natural tissue has autofluorescence and penetration depth of both visible light and UV are limited. Deep tissue penetration is crucial when in-vitro and in-vivo applications are considered. Lower chance of reflectance over blood makes NIR more convenient for optical imaging. Besides NIRQDs are usually excited in the visible wavelengths which is safe. Therefore, NIRQDs can be used for deep-tissue optical imaging as NIR I region between 650-950 nm is known as the diagnostic window.

1.2.4 QDs Developed In Our Group

Silver was used throughout the Roman Empire as drinking cups and therapeutic agents. Silver metal is well-known for its propensity to release silver cations inhibiting bacterial growth on metal surfaces. In recent years, silver in nano size has become quite popular to be evaluated in different applications.[40]

Ag metallic nanoparticle may be produced in varying size and shape such as bars, rods, cubic or spherical nanoparticles. According to the size and shape, its optical properties, antibacterial activity, conductivity, surface electric charge, and crystallinity differs. For example, triangular-shaped Ag nanoparticles tend to disturb bacterial membrane within three different edges simultaneously thus provide a higher rate of cell death.[41]

At the nanoscale, large surface to volume ratio enhances release of silver ions which are toxic and may therapeutically be toxic. Increment in release of silver ions requires caution. Unlike Ag nanoparticles, Ag_2S quantum dots have been drawing attention due to their safe dose usage especially in biomedical applications. Ag_2S QDs have a solubility product constant ($K_{sp} = 6.3 \times 10^{-50}$) which is ultraslow.[42] This property secures the biomedical environment with the least amount of Ag ion release thus inhibits high toxicity. The band gap of Ag_2S QDs is about 1.6 eV and it is reported that it is much

higher than the bulk silver sulphide.[43] The reduction in its size leads to an increase in the band gap, providing better optical properties. Ag_2S QD also has an emission range of 700-900 nm, making it the NIRQD that provides deeper tissue imaging and bypasses tissue background autofluorescence.[44]

Having a slow K_{sp} constant, Ag_2S QDs tend to form aggregates, however, they can be stabilised with a coating and endure well-controlled size distribution.[45] Coating can boost colloidal stability. Surface passivation, the chain length of the ligands and the particle size can effect colloidal stability. [46] Thiolated organic molecules are best suited for coating Ag_2S QDs. Di or multifunctional organic molecules with -SH functionality both binds to the QD crystal surface and provide surface functionality on the periphery.

As promising candidates for the fluorescent probes, NIRQDs are stable for long period of times and not prone to quenching. Having specialized in NIRQD production, our group developed the largest aqueous and stable Ag_2S QD portfolio in the literature.

Anionic Ag_2S QDs in our group have 2-mercaptopropionic acid (2MPA), N-acetyl cysteine (NAC) and Glutathione (GSH) as coatings. They have high stability with strong NIR luminescence and high biocompatibility. 2MPA and GSH coated NIRQDs were also shown as promising PTT agents and demonstrated ALA delivery for PDT/PTT combination. GSH coated NIRQDs achieved a dose dependent decrease in cancer cell viability with a safe laser irradiation at 795 nm, 700 mW and 1.8 Wcm^{-2}.[47]

Cationic Ag_2S QDs were also successfully synthesized using polyethyleneimine (PEI) and 2MPA mix as a coating.[48]

1.3 Proposal and Aim of This Thesis Work

Although cancer is the second leading cause of mortality after cardiovascular disease, bacterial infections also exhibit a growing concern especially due to increasing antibiotic resistance. [49] Bacterial infections can grow in many organs such as lung, liver, breast, colon, prostate, but especially in wound related tissues. Antibiotic resistance of biofilms is one of the major problems to be solved. As drug penetration through biofilm is insufficient, alternative approaches can be preferred eradicating the biofilms and killing bacterial infections. Concerning these issues, conventional therapies may have problems such as hypoxia, inaccessible location, malicious side effects, and low tendency in various immune system responses, thus, at the end, result in risk of metastasis or relapse.[50] Photo-mediated therapies emerge as highly efficient methods consisting of generation of

ROS and local heat. Although some of these therapies are potent, PDT, for example, needs the administration of a photosensitizer drug (PS). These drugs demonstrate poor colloidal stability, low solubility and are not entirely compatible with in vitro environment.[51] As a supporting step, there are nanoparticles for delivering PS to the bacterial cell. Several nanoparticles can be applied together with PTT to breakdown the biofilm or they can deliver drugs directly to biofilms. [52] Nanoparticle assisted antimicrobial photothermal therapy (aPTT) is locally effective and promising alternative for conventional ways to eradicate bacterial infections and biofilms. As shown in the Figure 2.1, nanoparticles exhibit valuable features such as high cellular uptake, deep tissue penetration and immediate inducement of killing mechanism of cells.

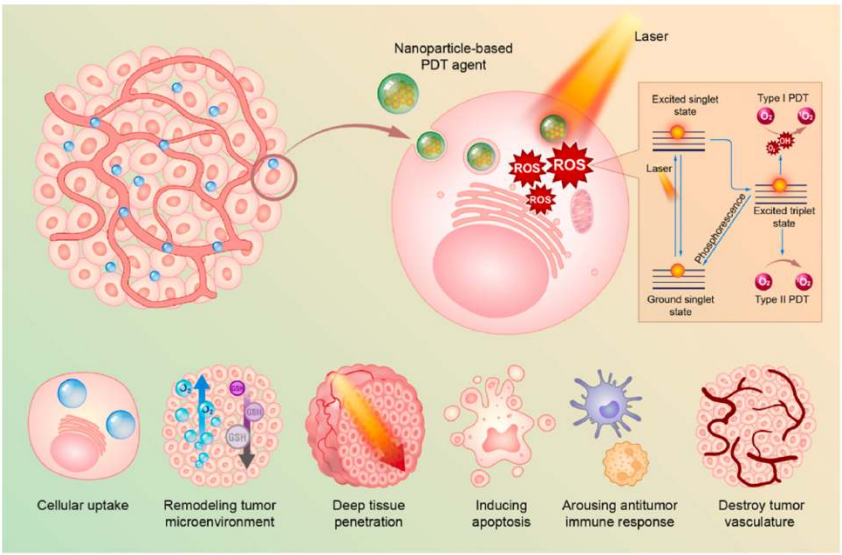

Figure 1.7: Nanoparticle mediated PTT and PDT scheme

PTT advantages inorganic nanoparticles such as Ag_2S QDs and SPIONs. They can successfully convert light energy to heat. SPION as a powerful MRI agent can provide information about the location and size of the tumour, but can also induce enhanced PTT and aPTT. SPION is the only magnetic nanoparticle approved by FDA, thus safe *in vitro* and *in vivo* application. Ag_2S QDs are well-operating in the creation of optical contrast especially during the operation. A hybrid nanoparticle composed of Ag_2S QDs and SPIONs would propose a dual imaging modality and PTT potential. This thesis aims to design and develop such hybrid nanoparticles with acceptable light-to-heat conversion efficiency, optimal hydrodynamic size that is even below 150 nm and strong luminescence to be utilised as theranostic nanoprobes.

Hybrid nanoparticle of such character embracing various functionalities may be prepared by an aqueous/organic extraction utilizing ligand exchange as described previously by Kas et al., 2010. [24] Electrostatic binding of QDs and SPIONs with opposite surface charges. The synthesis methods of hybrid nanoparticles described in this thesis are aimed at receiving optimal properties with both of these approaches. Many different hybrid nanoparticles with a variety of initial NPs were produced and characterized in Chapter 2.

Ag_2S QDs have been used as PTT and PDT agents *in vitro* by our group. ALA, a well-known prodrug with FDA approval, loaded QDs are also tested in vitro for PTT and PDT combination therapies. ALA is converted into into a well-known photosensitizer with red fluorescence Protoporphyrin IX (PpIX) in the mitochondria in the heme biosynthesis pathway. PpIX is not only used for PDT but also for diagnosis. Major limitations of ALA is the lack of stability and quick body clearance which may be solved by a nanoparticulate delivery vehicle that may stabilize ALA and effectively deliver it to the tumors to provide PpIX at a therapeutic dose. [53] Our group studied the effects of nanoparticle mediated PTT and PDT with ALA. This approach can be expanded to seek further enhancement of the eradication of the biofilm. NAC coated Ag_2S QDs were successfully synthesized by Buz et al., 2019 but not investigated for PTT potential.[54] Additional antibacterial activity of NAC was also reported but not studied as a coating for a QD. One of the proposals of this thesis is the improved treatment of antibiotic resistant, burn wound related biofilms by enhanced PTT/PDT provided by ALA loaded NAC coated Ag_2S QDs. Testing this hypothesis, Pseudomonas aeruginosa was made to infect a burn wound and then at the local scale of the wound different fluence rates of 640 nm laser were studied to trigger PTT/PDT in Chapter 3.

Chapter 2: Development of Hybrid Nanoparticles

2.1 Introduction

Synergistic hybrid nanoparticles draw a great interest due to their multifunctional nature. Dual imaging and dual therapy applications are also of great interest in medicine. There are many hybrid nanoparticles generally with organic/inorganic components together with integrated functionalities.[55] Hybrid materials may inhibit possible drawbacks caused by initial particles and present combinatorial effects for the final nanoparticle. Combination of optical and MRI imaging along with PDT/PTT offers several advantages, thus QD/SPION combination is proposed here. Optical imaging has a distinct advantage of sensitivity and NIRQDs proposed in this thesis benefit from high penetration of light in tissues. Concerning the presence of SPIONs, MRI has high resolution at any level of depth, and it can back up mediocre resolution from optical imaging.

Anionic Ag_2S QDs coated with NAC and 2MPA are synthesized based on a protocol developed by our group. [56] [57] NAC, both as a demanding material and therapeutic drug, is used as a capping agent for Ag_2S QDs.[58] Even though, MPA is reported to be a volatile and carcinogenic material, 2MPA and 3MPA are explored as other alternative stabilizers which are known as safer and environmentally friendly materials.[56] In QD synthesis, reaction environment is kept at pH=7.5 due to presence of acetic acid and NaOH.[59] Arranging and monitoring pH of the solution is crucial as it affects aggregation and formation of possible precipitates. Therefore, it is excessively important in synthesis of NIR-emitting QDs as any aggregation on the surface influences an alteration in the luminescence.[59] For example, if there is a precipitation formed in the solution, it gradually lowers the luminescence of QD. Acidic or basic environment is directly related to photoluminescence quantum yield, PLQY, percent of QDs. PLQY % and fluorescence intensity are changed to a great extent when pH, thus, size of the QDs alter. pH leading to different precursor solution acidity results in an adjustment of both absorption and fluorescence spectra as shown in the Figure 2.1.

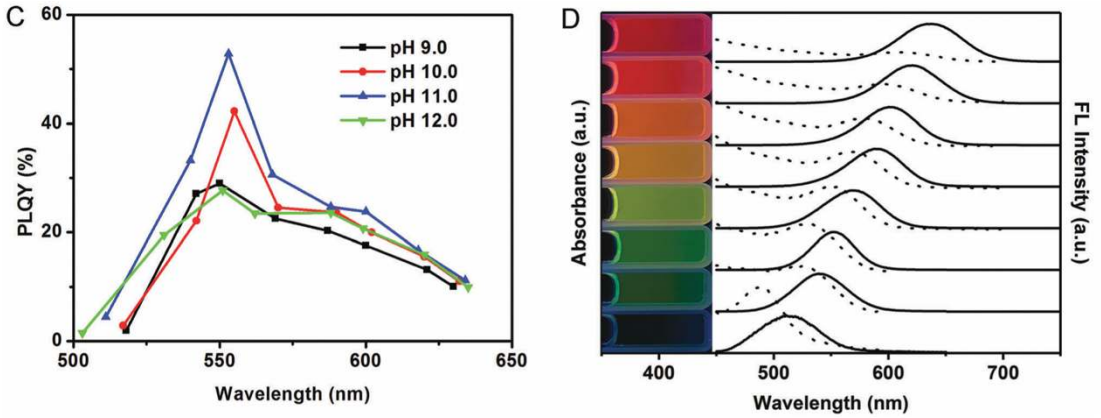

Figure 2.1: Adjustment of PLQY % and fluorescence [59]

SPIONs have different coatings, as well. As long as coating is covalently bonded and interacted well on the surface, the iron oxide core will stay stable for long amount of time. Magnetic nanoparticles instead of heavy metal ions are preferred for many reasons including large surface area and superparamagnetism. This alteration arises new challenges such as susceptibility of these nanoparticles to oxidation and congestion. That is why coating is vital when synthesis of SPIONs is considered. Protective layer, also called as a coating, is advantageous especially for chemical stability and dispersibility enhancement.[55] APTMS, as a common aminosilane, can be used for silanization process due to its silane functional groups. In this process, this molecule is used for covalent attachment of silane ending to a metal oxide.[25] Underlining the strength coming from this bond, silane is an efficient functional group to interact with an iron oxide core, in this scenario. Moreover, according to Palimi, surface treatment with APTMS resulted in cogent improvement of some mechanical properties. [60] APTMS coating was a convenient alternative in our synthesis procedure.

Our group synthesized and reported PEG, PAA, APTMS and LA coated SPIONs. Regarding the surface charges in this study, LA coated SPION is synthesized and transferred into organic layer of chloroform, PAA-SPION and APTMS-SPION are also synthesized. Cationic surface charges of APTMS and mono-layered LA-SPION are used to produce hybrids with anionic NIRQDs.

Although it is luminescent in the visible region and not NIR-emitting, a hybrid nanoparticle is synthesized composing carbon dots (CDOT) and SPION. In a research studying CDOTs, endowed magnetic features did not decrease photoluminescence but drastically enhanced its properties. CDOTs are more likely to experience such occasions since a new addition may be utilised to fill or generate new trap states in

surface of a CDOT.[61] Therefore, it may be enhancing the PL intensity. It serves an example to explore the possibilities since CDOT surface is functional and lacks an organic molecule as its coating. Cationic surface charge of CDOT is to coupled with anionic surface charge of PAA-SPION.

2.2 Materials and Method

2.2.1 Materials

PAA coated SPION was synthesized following a co-precipitation solvothermal method. FeCl2.4H2O and FeCl3.6H2O salts were purchased from Merck Millipore (MA, USA). Poly(acrylic acid) (Mw 5100 kDa) and dimethyl sulfoxide Hybri-MaxTM were obtained from Sigma (MO, USA). Lauric acid (LA) was purchased from Fluka. Ammonium hydroxide (26 %) was purchased from Aldrich (U.S.A.). Hydrochloric acid (37 %) was purchased from Carlo Erba (France). Acetic acid (99.8 %) was purchased from Lachema (Czech Republic). Vivaspin 20 centrifugal filters (5000 Da MW and 30 kDa MW cut-off) were obtained from Sartorius (Goettingen, Germany).

2MPA and NAC were the functional groups used for coatings in QD stabilization. 2MPA, ethanol and acetic acid (CH3COOH) were purchased from Merck (USA). Silver nitrate (AgNO3, 99.9999%) was purchased from Aldrich (MO, USA). Sodium sulfide (Na2S) was purchased from Alfa-Aesar (Lancashire, England). NAC, sodium hydroxide (NaOH), sodium chloride (NaCl), Suprapur nitric acid (65%) and Suprapur sulphuric acid (96%) were obtained from Merck Millipore (MA, USA). Vivaspin 20 centrifugal filters (3000 Da MW cut-off) were obtained from Sartorius (Goettingen, Germany).

2.2.2 Instruments

Shimadzu UV-VIS-NIR spectrophotometer was used to detect the optical transmission of the hybrid particles in the 300-10000 nm range in water. Samples were placed in 10mm quartz cuvettes. Malvern Zetasizer Nano ZS was used to quantify hydrodynamic size and zeta potentials. Thermo K-Alpha X-Ray Photoelectron Spectrometer was used to analyse the surface of both hybrid nanoparticles, SPIONs and QDs. Thermo Scientific iS10 FT-IR spectrometer was used to investigate functional groups in the wavenumber range of 650-4000 cm^{-1} with a resolution of 4 cm^{-1} against a water and, if feasible, air background. The particle sizes and shapes were validated using a Hitachi 7800 TEM. Cell viability was determined using a Synergy - H1 microplate reader from BioTek Instruments Inc. (Vermont, United States).

2.2.3 Preparation of NAC and 2MPA Ag_2S NIRQDs

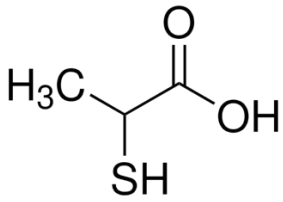

Figure 2.2: Chemical structure of 2-mercaptopropionic acid

There is an optimised standard to produce Ag_2S core QDs, while its coating can differ. Both NAC and 2MPA coatings were utilised based on the published procedure from our group with minor changes. Both NAC and 2MPA coatings can be utilised following a similar production technique. 75 mL of deionized, DI, water in a round-bottomed flask was purged under Ar. 111 ul of 2MPA was dissolved in water, still under Ar. Following the addition of 2MPA, pH of the solution was arranged to 7.5 adding 1M NaOH and 1M CH3COOH dropwise. 42.5 mg of AgNO3 was added to the same solution and caused a pH raise. Again, basic environment was adjusted to pH=7.5. Here, 4.9 mg of Na_2S was dissolved in a separate flask under Ar and later added to main reaction at room temperature (RT). Synthesis was carried out for 90 minutes. For NAC coated Ag_2S QDs, $AgNO_3$ and NAC were added in distilled water and dissolved respectively. Reaction takes place in a round bottom flask for the ease of heat conduction as the reaction environment is gradually heated to 80 ºC degrees. Na_2S is dissolved in a separate flask under Ar and later added to main reaction at 80 ºC degrees. NAC-coated Ag_2S QD synthesis took 30 minutes. Both syntheses were performed at vigorous mechanical stirring at 500 rpm. QD solutions were pale brown coloured and washed with DI water several times until their solutions were concentrated enough. 3 kDa MWCO Vivaspin centrifugal filters were used to wash the solutions and to remove excess unreacted molecules. QDs were stored in the dark at 4 °C.

2.2.4 Preparation of APTMS, LA and PAA coated SPIONs

Like a fundamental SPION synthesis protocol, APTMS coated SPION was synthesized following a co-precipitation method from two different iron salts. [Fe3+]: [Fe2+] = 2:1 ratio is an important parameter both to seek for co-precipitation of iron salts and synthesize magnetite nanoparticles. Iron salts were added in pH=10, with 8,33 mmol

and 4,1675 mmol for $FeCl_3$ and $FeCl_2$ respectively. Salts were stirred inside a round bottom flask and dissolved. The reaction mixture was located inside an oil bath which is set to 85°C. When dissolving of substances was finished, reaction temperature was allowed to raise accordingly. APTMS and NH4OH (7,89 ml) were mixed under Ar in a separate round bottom flask. This solution was injected into the main reaction flask at vigorous stirring at 600 rpm. Enduring a steady temperature, the reaction mixture persisted for an hour to obtain colloidally stable solution. The particles were acidified with a small amount of acetic acid to endure its cationic environment. Right after it was cooled down at room temperature, the reaction mixture was placed on top of a magnet to remove any precipitated particles at the bottom and washed with three times more of its volume. Washing through 30 kDa MWCO Vivaspin 20 centrifugal filters, with DI water was maintained to discard any impurities. At the end, APTMS-coated SPION was stored at room temperature.[62] [26]

PAA and LA coated SPIONs were synthesized following almost the same similar procedure. Coating materials were introduced directly to the main reaction flask, with no degassing required in a separate round bottom flask. Similarly, after dissolving iron salts with vigorous stirring, LA and PAA components were added immediately to the reaction mixture and well mixed with the iron salts. Another distinction is the selection of Vivaspin 20 centrifugal filters (5 kDa MWCO).[63] [64] All three coatings have different sizes, thus, impurities or materials that did not participate at the reaction formation need to be removed through different pore sizes. As the pore size of a centrifugal filter is decided upon the nanoparticle size in a solution, some SPIONs are washed with different filters. For example, molecular weight of PAA is 5100 kDa, so unreacted PAA is removed via 5 kDa MWCO centrifugal filters. Therefore, after an overnight waiting on top of a magnet, LA-coated SPION was washed with 10 kDa MWCO Vivaspin 20 centrifugal filter.

2.2.5 Preparation of Hybrid Nanoparticles

Hybrid nanoparticles can combine two modalities in a single entity to encompass synergistic effect. This thesis focuses on providing sensitivity and high resolution in medical imaging with a collaboration between SPION and QD. These materials can be synthesized via tuning SPION/QD ratio.[24] This facile modification can be performed via two different methods such as titration and extraction. So, single step synthesises are presented.

2.2.6 Hybrid Nanoparticles Through Extraction

Extraction is a facile method that signifies ligand exchange mechanism. In hybrid synthesis, there are two steps regarding the extraction. LA-coated SPIONs were synthesized within a bilayer coating. LA coated SPIONs were extracted into chloroform as LA monolayer coated SPION. 1 ml of SPION (generally around 40 mg/ml) and 3 ml of chloroform were added in a vial together with 900 ul of isopropyl alcohol, IPA. Solution was taken to sonicator for a few minutes and then shaken vigorously until layers were separated efficiently and qualitatively. SPION at chloroform layer was dried to measure its concentration, then transferred into another vial later to be utilised in hybrid synthesis. Concentration of monolayer LA-coated SPION was measured again since it was expected to be lower than that of in previous solution and to change in a different solution.

Monolayered LA-SPION in chloroform was extracted with a QD in aqueous solution. Both NAC and 2MPA coated QDs were used in this experiment. At first trial, equal volumes of both SPION and QD were mixed in a round bottomed flask and sonicated briefly at room temperature. Reaction mixture was set to shake at 500 rpm for 2 hours. At the end of an hour, most of the extraction was performed. The mixture was transferred into a separatory funnel which was designed to separate aqueous and organic layers. Colourless organic layer was separated, and the aqueous phase was supposed to contain hybrid nanoparticles. The aqueous phase was endured a back-extraction with chloroform to lead unmodified monolayered SPION particles back to the organic phase.[24] So, if they were not in the hybridized form interacted with QDs, they were supposed to be placed in the organic phase. The prerequisites for a successful extraction were first grasped qualitatively. Given that the chloroform solution remained colourless, all SPIONs were transferred to the aqueous phase, as the dark colour was produced by the presence of SPION. Back extraction was conducted twice. Hybrid solution was washed again from 10 kDa MWCO Vivaspin 20 centrifugal filter. Washing was continued until there was no more luminescence in the solution. Hybrid nanoparticles were filtered again from 200 nm aqueous syringe filter. According to Kas et al. (2010), two stock solutions both for QD and SPION were prepared to alter Ag/Fe ratio during the extraction. 5, 10, 15, 20 mL of iron oxide stock solution was prepared and mixed with 30 mL aqueous QD at a 2.5 mM Ag concentration.[24] In this set of experiments, QD concentration was kept same while iron oxide amount was changed.

2.2.7 Hybrid Nanoparticles Through Titration

Anionic QDs and cationic SPIONs may be electrostatically bound to produce a hybrid structure. To determine the maximum binding capacity, isothermal titration calorimetry, ITC (Affinity ITC, USA) seeks a saturation over exotherms. Also, titration experiment minimizes the percent errors and present a model of exact binding through exotherm peaks. Enthalpy changes during titration were observed due to electrostatic interaction between QD and SPION. Higher concentration of both QDs (10 mg/ml) was prepared in the syringe and titrated on SPION (1 mg/ml). AS-2MPA QD was injected on APTMS-SPION at the rate of 15 µL/s.[31] Throughout the experiments, the temperature of the solution in the titration cell was kept fixed at 25 °C. After each injection, the data are provided as the change in enthalpy per titration (cal) vs the concentration of injected QD. Exotherms were demonstrated to confirm binding and the end point of binding between anionic AS-2MPA QD and cationic APTMS-SPION, but no clear end point suggesting a saturation point was reached. In real time titration, the experiment was conducted without any precipitation observed, thus, it was still evident for us to seek all nanoparticles were intact in means of electrostatic interaction. The hybrid nanoparticle was not washed after the electrostatic loading of 250 ul of AS-2MPA QD to 1 ml of SPION solution.

Another type of a hybrid material was prepared by titrating anionic PAA-SPION with cationic CDOT produced by Ahmet Ferid Fırat (unpublished). PAA-SPION concentration was set at 0.05 mg/ml, whereas CDOT concentration was allowed to change between 0.05 mg/ml and 1 mg/ml. As difference between titrant and the substance that is being titrated varies, it is estimated to have a better grasp of interaction. Hybrid combination of these two particles was a promising candidate to establish higher penetration in living cells due to its red-emissive character and potential effectiveness in photo thermal therapy as well as its highly biocompatible nature.

2.2.8 Hybrid Nanoparticles

Overview of Hybrid Synthesis			
		Initial NPs used in the hybrid synthesis	
Hybrid Code	Method of synthesis	SPION	QD or CDOT
Hybrid 1	Extraction	LA	AS-2MPA-QD
Hybrid 2	Extraction	LA	AS-NAC-QD
Hybrid 3	Titration	APTMS	AS-2MPA-QD

Hybrid 4	Titration	APTMS	AS-NAC-QD
Hybrid 5	Titration	PAA	CDOT

Table 2.1: A portfolio of hybrid nanoparticles synthesized either via titration or extraction methods

Hybrid Type 1 and Hybrid Type 2 were synthesised following the procedure described by Hocaoğlu et al., (2015). [65] As shown in the Table 2.1., Hybrid Type 1 and Hybrid Type 2 consisted of AS-2MPA-QD AND AS-NAC-QD respectively. Both consisted of LA-SPION in chloroform. First optimization was carried out for Hybrid Type 1 and then carried out for Hybrid Type 2. The goal here was to obtain hybrid with different Ag/Fe ratio to tune the luminescence and PTT efficiency while keeping the size small and maintain colloidal stability.

For some of these trials, extraction was successfully followed as chloroform and aqueous layers were qualitatively separated at first. Some of the trials were exposed to a difficulty of sticking to the interphase layer of the extraction. Changing dilutions of both QD and SPION in volume basis, different ratios were examined as it was shown in Table.2.2.

			LA-SPION to Chloroform dilution			
AS-2MPA-QD to Water dilution	**Concentration of the stock QD**	**Dilution ratios**	**1**	**1-1 dilution**	**1-2 dilution**	**Concentration of the stock SPION**
	9 mg/ml	No dilution	Hybrid 3	Hybrid 5	Hybrid 1	55 mg/ml
		1-1 dilution	Hybrid 4	Hybrid 6	Not extracted	
		1-2 dilution	Hybrid 2	Not extracted	Not extracted	
		1-6 dilution	Not extracted	Not extracted	Not extracted	
		1-12 dilution	Not extracted	Not extracted	Not extracted	

Table 2.2: First optimization of Hybrid Type 1 and Hybrid Type 2

2.3 Results and Discussion

2.3.1 Characterization

Our goal was to create both superparamagnetic and luminescent hybrid nanoparticles, but we acknowledged that the potential hybrid would be less superparamagnetic because ligand exchange may cause some surface dead layers and magnetic content would be lower in the hybrid. Additionally, final hybrid NP would be less photoluminescent because it would be quenched due to high absorbance of SPION and may be due to proximity of QDs.

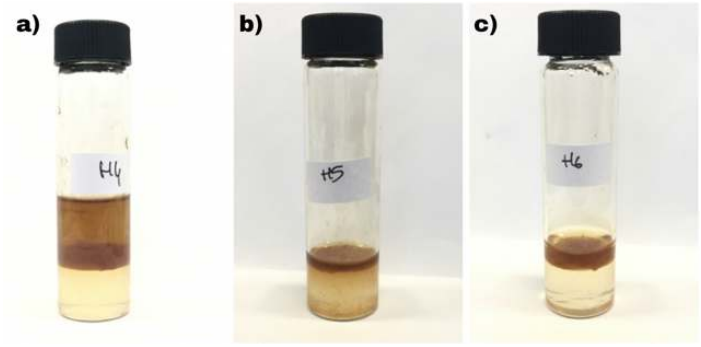

Figure 2.3: Extraction and interphases of different particles at optimization (a-c)

These hybrid nanoparticles and their last three washing water solutions were characterized, first with UV Spectrometer, PL, dynamic light scattering, DLS-Zeta Sizer. Out of all trials, two of the most luminescent hybrid NPs were selected as the best hybrids. DLS-Zeta Sizer was a convenient characterization method for measuring the hydrodynamic sizes of the nanoparticles. Hybrid nanoparticles were bigger than both QD and SPION as expected in Table 2.3. Two of the most stable hybrid nanoparticles were synthesized repetitively fulfilling the need for reproducibility. Like in Figure 2.2. (a-c) the most transparent organic layer was thought to give the most stable hybrid nanoparticle as the more it gets transparent it means there is less SPION, almost no SPION, in organic layer.

	Hybrid Sample Name	Size (d.nm)		Zeta Potential (mV)	Concentration (mg/mL)	QD used					SPION used				
		by Number	by Intensity			Name	Concentration (mg/mL)	Size by Intensity	Size by Number	Zeta Potential (mV)	Name	Concentration (mg/mL)	Size by Intensity	Size by Number	Zeta Potential (mV)
2MPA-LA-Hybrid	EC416	88,21	251,2	-23,8	5	EC016	30	9,896	4,007	-44	EC04	4	36,91	16,09	-40,5
	EC420	200	232	-47,1	3	EC020	29	2,939	0,8317	-18,6	EC04	4	36,91	16,09	-40,5
	EC518	79,75	158,9	-19,5	13,4	EC018	26,6	3,522	2,546	-61,7	EC05	6	59,87	17,1	-53,7
	EC712	24,93	74,89	-8,36	6,2	EC016	30	9,896	4,007	-44	EC05	6	59,87	17,1	-53,7
	EC518 (diluted)	48,5	143,9	-36,2	6,2	EC018	26,6	3,522	2,546	-61,7	EC05	6	59,87	17,1	-53,7

Table 2.3: Comprehensive comparison of Hybrid Type 1 characterization

	Hybrid Sample Name	Size (d.nm)		Zeta Potential (mV)	Concentration (mg/mL)	QD used					SPION used				
		by Number	by Intensity			Name	Concentration (mg/mL)	Size by Intensity	Size by Number	Zeta Potential (mV)	Name	Concentration (mg/mL)	Size by Intensity	Size by Number	Zeta Potential (mV)
NAC-LA-Hybrid	EC421	570,2 (1)	779,5	-60,2	26	EC021	27	4,019	2,51	-35,4	EC04	4	36,91	16,09	-40,5
	EC417	3,968	4,709	-60	10	EC017	34	4,674	3,005	-49	EC04	4	36,91	16,09	-40,5
	EC419	27,66	32,16	-69,6	17	EC019	30,6	5,421	2,468	-81,9	EC04	4	36,91	16,09	-40,5
	EC519	47,36	183,2	-9,93	18	EC019	30,6	5,421	2,468	-81,9	EC05	6	59,87	17,1	-53,7

Table 2.4: Comprehensive comparison of Hybrid Type 1 characterization

For anionic particles, zeta potential should be very low so that it can be ensured that the whole particle is without any aggregates or sedimentation[66] is covered with negatively charged functional groups. Similar zeta potential values should be considered for equally monodispersed nanoparticles. In Table.2.3 and Table2.4, different hybrids with varying zeta potential values mean that obtained nanoparticles are not repeatable. Especially, EC712 is not a very stable nanoparticle with encapsulation of anionic QD of -8,36 eV zeta potential. Likewise, information on size is also not consistent with all trials. EC518 and EC416 are similar nanoparticles and consistent with the data that is obtained from literature.

Initial characterization of the hybrid NPs involved determination of PL and absorbance characteristics. PL and absorbance spectra of 2MPA coated Ag_2S QDs are shown in Figure 2.3. PL Absorbance calibrated PL intensity of Hybrid Type 1 and 2 in was compared to their respective QDs in Figure 2.3. c). Hybrid Type 1 showed an expected decrease in PL intensity whereas Hybrid Type 2 did not demonstrate such relation. This result was not expected and did not correlate with previous results. Previously, Hocaoğlu et al. (2010) also showed a synthesis of hybrid NP composed of AS-2MPA-QD and LA-SPION through extraction and PL intensity decreased in hybrids. [65]

Hybrid had the highest PL intensity compared to PL intensity of washing water solutions as it was shown in Figure 2.3. d). This result was expected and was in comparison with absorbance graph of Hybrid replicas shown in Figure 2.3. e). Absorbance calibrated PL intensity was in accordance with PL and absorbance graphs of

AS-2MPA-QD shown in Figure 2.3. (a, b, f).

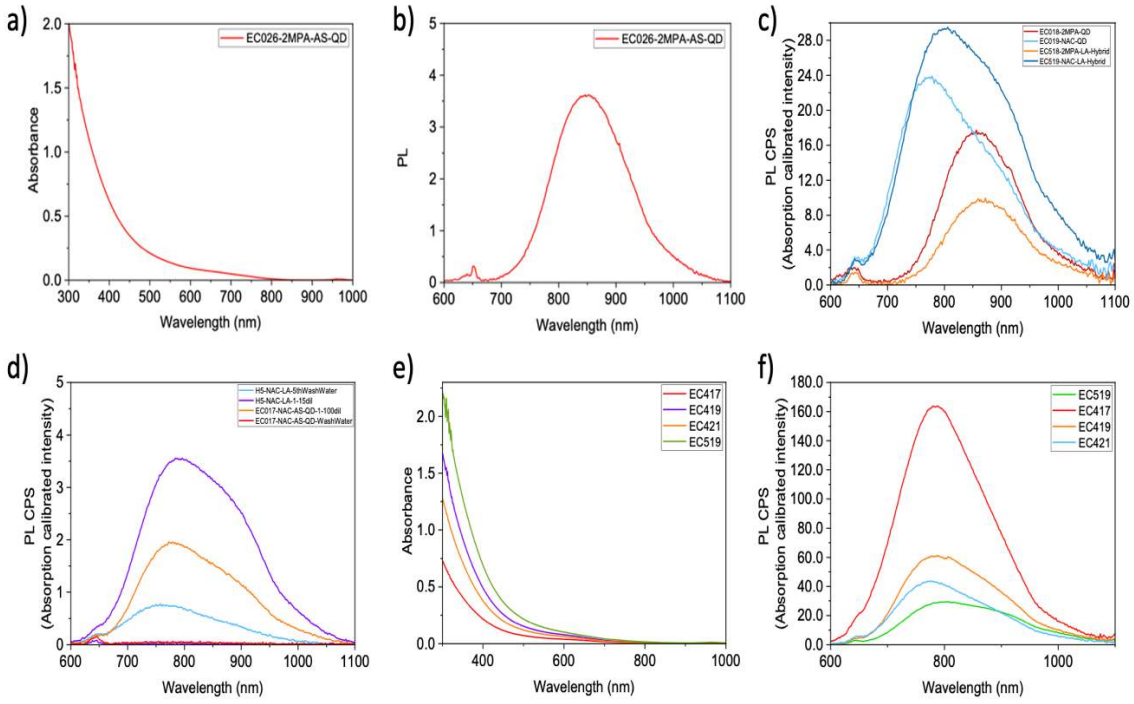

Figure 2.4: Absorbance of AS-2MPA-QD (a), PL graph of AS-2MPA-QD (b), Absorption calibrated PL intensity of Hybrid Type 1 and Hybrid Type 2 (c), Absorption calibrated PL intensity of washing waters and AS-NAC-QDs (d), Absorbance of different replicas of Hybrid Type 2 (e), Absorption calibrated PL intensity of Hybrid Type 2 (f).

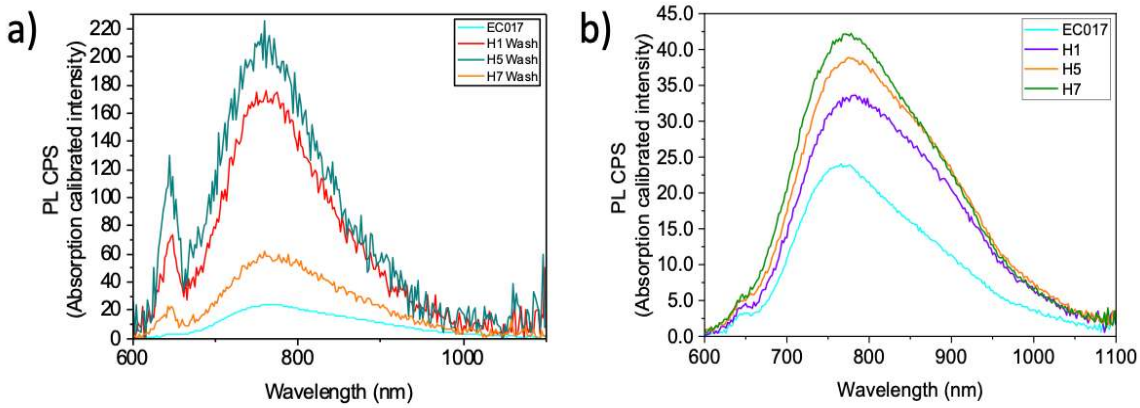

Figure 2.5: PL intensity of washing water solution compared with AS-NAC-QD (a), PL intensity of Hybrid Type 2 compared with AS-NAC-QD (b)

Figure 2.3. showed PL of many washing water solutions in comparison with QDs. Washing waters exhibited a lower level of PL since QDs unbounded to the hybrid structure left the solution while washing. It was in accordance with the expectation.

However, Figure 2.4. a) showed PL intensity of washing water solutions had the highest PL intensity meaning that most of the QDs are washed away from the solution. This claim implies that the experiments did not function. Moreover, similar problem was present in Figure 2.4. b) exhibiting PL intensity of AS-NAC-QD with comparison of Hybrid Type 2. PL intensity was not lower than that of QD as it was the case in previous results.

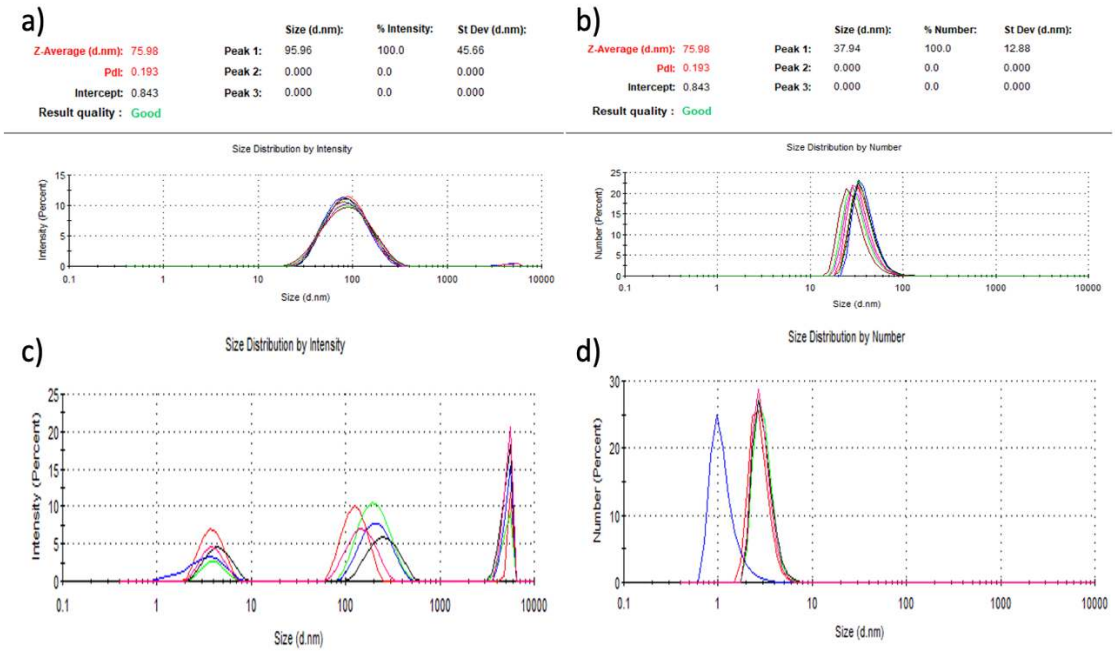

Figure 2.6: Size Distribution by Intensity and Number of Hybrid Type 2 (a-b) and Hybrid Type 1 (c-d)

As Hybrid Type 2 demonstrated a monodisperse size distribution as shown Figure 2.5. (a-b). It was not always repeated and caused reproducibility problems. Additionally, it was also problematic for Hybrid Type 1 not to have a monodisperse size distribution because at the end two synthesis procedures were very parallel to each other.

In many respects, including the application field, the production of a monodisperse nanoparticle[67] is essential. Drawing a huge attention towards the relationship between NP structure and property, monodisperse nanoparticles have tuneable size and controllable properties linked to that. Such particles are uniformly packed, not prone to aggregate as they exhibit a sense of self-assembly. These chemical properties are significant for a particle to own biodistribution[68] effects. As a result, we anticipated that our nanoparticles will be monodisperse to the greatest extent possible. Additionally, size and PL are directly related as it is exhibited in a study[69] regarding particle size, distribution of the particles and PL peaks of QDs. In this study, absorption of incident

solar radiation through different sizes of QDs, measured via transmission electron microscope, TEM, results in an excess of charge carriers which then has an increase in the photoelectric current.

Finally, EC019, an AS-NAC-QD example, and EC519 hybrid underwent a solution heating test using 640 nm, 215 mW LED irradiation for 20 minutes. QD and hybrid nanoparticles were produced at concentrations of 10, 50, and 100 ug/mL. 100 ug/mL of Ag in EC519 resulted in 2,72084 °C temperature increase whereas respective Ag amount in EC019 AS-NAC-QD arose 2,62812 °C increase. In a comparable manner, 10 mg/mL Ag of the same hybrid produced a temperature rise of 0,2551 °C, whereas the same quantity of Ag in its QD followed a temperature increase of 0,37247 °C.

Figure. 2.6 showed a result indicating that, although the opposite was anticipated, QD heated more than hybrid. This situation suggests that a hybrid design was not successful, as some of the Fe quantity was somehow trapped in the interphase and not all of it was directly transferred to the aqueous phase surrounded by QDs. This led to fluctuations in Fe and Ag amounts, Ag/Fe ratios resulting in an inconsistency in hybrid production. If there would be more Fe transferred to the aqueous layer, it would assist heating to a greater extent as it was known that SPION has a huge heating potential in this absorbance interval as it was reported in our group.[26]

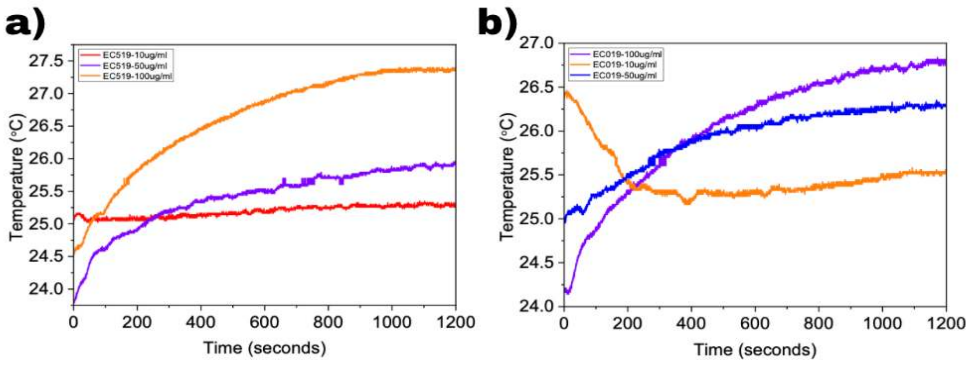

Figure 2.7: Solution heating results of QD and Hybrid Type 2

As previously stated, titration would be preferable than extraction. Hybrid Type 3 and 4 were produced to increase Ag and Fe enactment. Therefore, Fe amount in a hybrid would increase and eventually lead to a better heating. Also, controlling Fe amount in a hybrid nanoparticle was difficult in extraction procedure compared to titration. Therefore, Fe addition to the hybrid nanoparticle would be better since there would be no interphase that the SPION can be trapped in. A further problem that arose in Hybrid Type 3 and

Type 4 was the potential danger of SPION precipitation. With an increasing amount of SPION content in a simple titration, there is a risk of precipitation of the nanoparticle. Electrostatic loading implies a significantly more concentrated QD solution in the syringe, whereas electrostatic loading requires a substantially less dilute SPION concentration in the cell. For the final nanoparticle not to be precipitated, Fe amount coming from SPION would not be high as much as it was intended.

Hybrid Type 3 and Hybrid Type 4 were prepared by titration of cationic APTMS-SPION with anionic AS-2MPA QD and AS-NAC QD. Hybrid Type 4 was studied but precipitated in every trial. That is why, in this section Hybrid Type 3 was mostly studied and.

According to ITC exotherms 250 ul of AS-2MPA-QD loading did not reach a saturation point. So, any Ag/Fe ratio at and below this one should produce a hybrid nanoparticle via electrostatic interactions. As shown in Figure 2.7, 3 different QD loadings were investigated. QD loading with 63,31% and 81,30% were the most luminescent ones as exhibited in Figure 2.7. f). Their PTT potentials were investigated in Figure 2.7. (b-c), however, they could not achieve more temperature rise than AS-2MPA-QD did.

a)

Sample Code	QD Weight %	Intensity (d.nm)	Number (d.nm)	Zeta Potential (mV)
V1	63,31	176.3	131	-48.5
V2	81,30	141.4	21.99	-34
V3	51,80	309.8	53.07	-32

b)

Sample Code	QD Weight %	Ag amount (ppm)	Temperature Rise (°C)
Control (Only Water)	0,00	0	1,859
Only QD	100,00	50	**3,630**
V1	63,31	50	2,196
V2	81,30	50	1,525
V3	51,80	50	1,660
Only QD	100,00	500	**8,269**
V1	63,31	500	4,591
V2	81,30	500	3,713

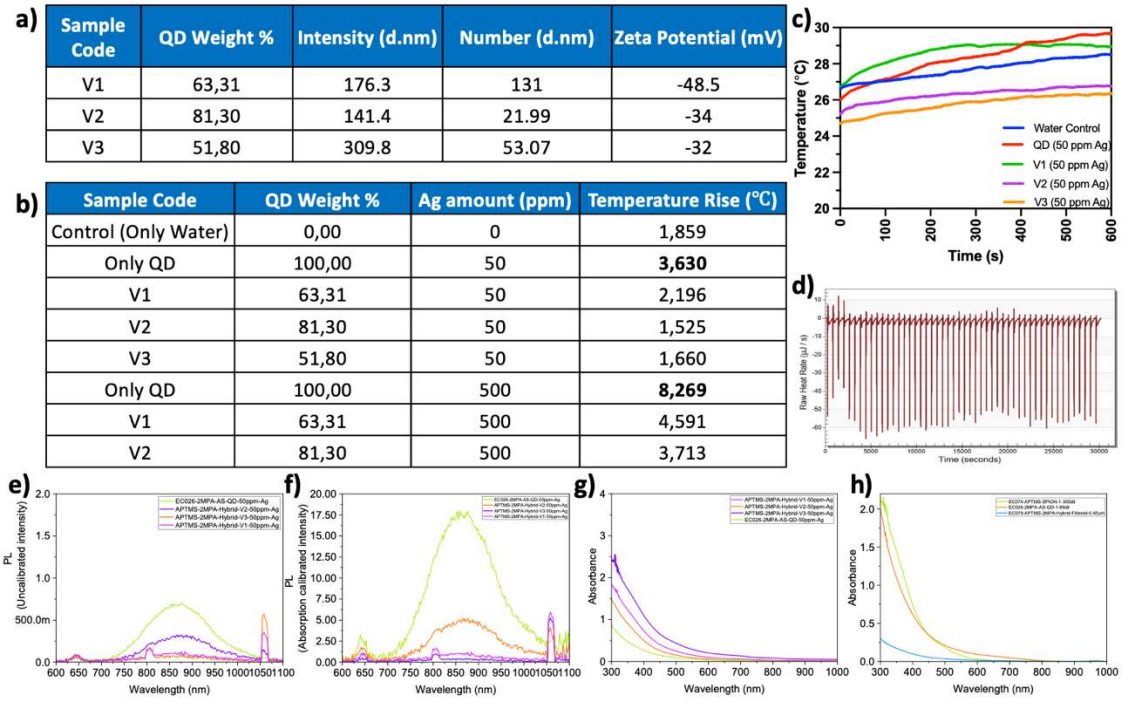

Figure 2.8: Size, zeta potential, QD percentage of different versions of Hybrid Type 3 (a), Temperature rise of different versions with same Ag ratio (b), Solution heating graph of Hybrid Type 3 via LED irradiation (c), Titration of AS-2MPA-QD on APTMS-

SPION (d), Uncalibrated PL intensity of Hybrid Type 3 with same Ag ratio (e), Calibrated PL intensity of Hybrid Type 3 with same Ag ratio (f), Absorbance of Hybrid Type 3 with same Ag ratio (g), Absorbance comparison of Hybrid Type 3, APTMS-SPION and AS-2MPA-QD (h)

DLS results of these hybrid did not establish an aggregated sample in Figure 2.7. a). In Figure.2.7. c) heating potentials of hybrid with a varying percentage of QDs at a fixed concentration of Ag under 640 nm, 215 mW, LED irradiation. It did not demonstrate more temperature raise in hybrids. Figure 2.7. b) showed that only AS-2MPA-QD showed a temperature rise of 8,269 °C while Hybrid version 1 showed a difference of only 4,591°C. Analysing solution heating observations from all perspectives led to the conclusion that QD heated more efficiently than the hybrid.

Hybrid Type 5 was considerably more instantly superparamagnetic and luminescent when compared to other nanoparticles. Superparamagnetism from the SPION and its additive feature as a luminescent nanoparticle from the CDOT manufactured a dual-functioning hybrid nanoparticle. CDOT presence probably induced a much more stable nanohybrid formation. Carbon presence generally brings surface passivation schemes [70], [71] to the nanoparticles that they are doping. Surface passivation around SPION might have been effectively utilised as a stabilizing factor for the hybrid nanoparticle production. PL intensity was extensively high as in 800 a.u. in the spectra whereas its absorbance was 1/10 of an unreacted PAA-SPION as in Figure 2.10. CDOT amount was fixated and SPION amount was subjected to differ. As in first version of Hybrid Type 5, CDOT/SPION ratio was 3,6 while at the third version this ratio altered as 1,2. Furthermore, as compared to other hybrids, Hybrid Type 5 has greater CDOT encapsulation and higher stability. Having an endpoint in an ITC graph may indicate a little shorter end for electrostatic interactions, but it may not represent a continuous flow of electrostatic interactions. In other titration hybrids, exotherms on ITC graph were

continuous in a way that nanoparticles were in a complex system.

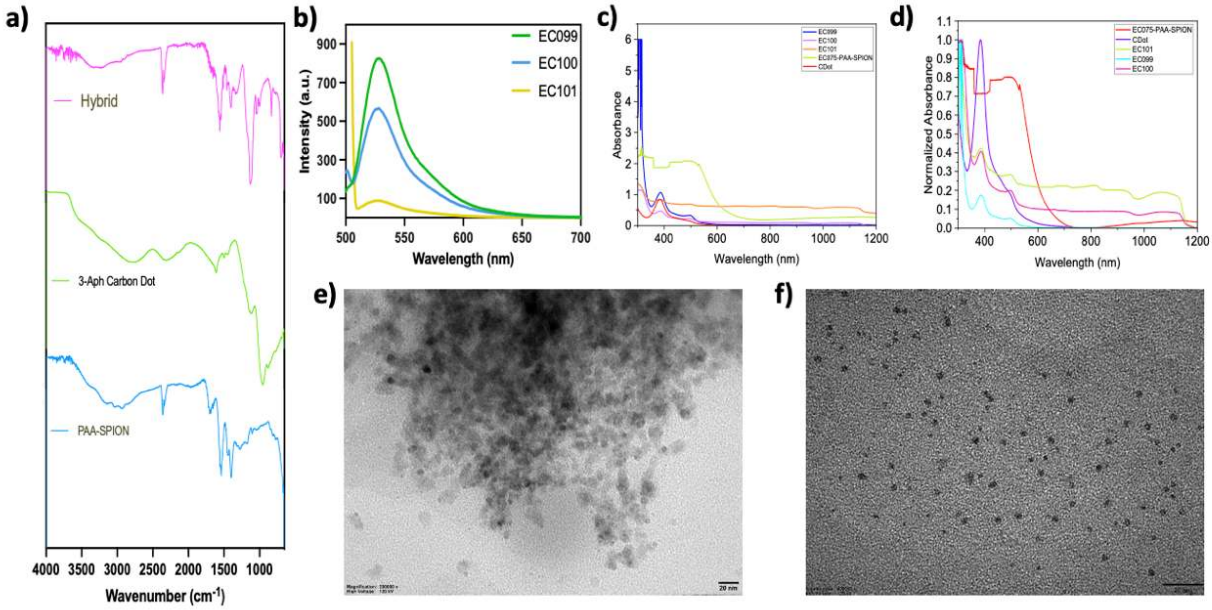

Figure 2.9: FTIR spectrum of CDot, SPION and Hybrid NP Type 5 (a), PL graph of different versions of Hybrid Type 5 based on 500 ppm SPION (b), Normalized absorbance and absorbance graph of different hybrid NPs in comparison with PAA-SPION and CDOT (c-d), TEM image of Hybrid Type 5 and CDOT (e-f)

TEM images reveraled that phosphoric acid containing CDOT alone was monodisperse, however, Hybrid Type 5 established a muhc more dense electronic interaction over a nanoparticle. This condition can easily be seen via TEM imaging in the Figure.2.8 d). Contrast intensity is highlighted when it comes to SPION presence and somehow emmerged within CDOTs.

2.4 Conclusion

Superparamagnetism and photoluminescence are an intricate pair that provide many obstacles and need a sweet spot to work well together. Ag/Fe ratio alters with a high standard deviation so that a reproducible result cannot easily be achieved through. Stacking in between phase transfer layer would be causing many problems as SPION in organic layer would not be transferred efficiently to the aqueous phase. Compared to QD usage in hybrid nanoparticle production, CDOTs have advantages in terms of stability and electrostatic environment. Unpaired electrons[72] from CDOT to the hybrid structure have been resolved in means of obtaining magnetic properties. Results from this chapter showed that several features in CDOTs provided hybrid nanoparticles a more stable

nature as well as optical properties so that these materials would be efficiently utilised in photocatalytic and catalytic activities. Moreover, sensing applications can be enhanced with Fe ion presence in the hybrid NP production so that SPION core can detect several molecules apart from those that are already in applications.

Chapter 3: Eradication of Wound-related biofilms via mild PTT using NAC coated Ag_2S NIR-QDs

3.1 Introduction

Infection on a wound is an important complication that can easily occur on a skin. Whenever a bacterium or a pathogen enters a wound, an infection appears. A simple symptom of a wound infection can be pain, swelling or redness.[73] Type of the treatment generally depends on severeness of the wound. Minor wound infections can easily be treated at home; however, wound healing rises an urgent problem nowadays. Wound-related infections and poor wound healing affect many individuals worldwide. It also increases mortality rates and its related costs while accounting for the third most common cause for death overall the world. [74]

Wounds have main key aspects such as having an inadequate space to allow cell migration, microbial infection and unstable inflammation. [75] Those three obstacles may have contemporary solutions; however, bacterial biofilms can be much more resistant to conventional therapies. Bacterial biofilm has a different mechanism that easily develops resistance. This is due to exopolysaccharides inhibiting the degradation and inactivation of antibiotics. Furthermore, deep seeded cells into the biofilm may be inaccessible to antibiotics.[76]

Antibacterial agents that are mostly based on nano silver materials possess a wide spectrum of advantages due to their potent structure.

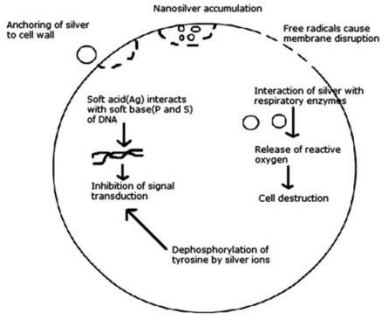

Figure 3.1: Various modes of Ag-based nanoparticles for bacterial applications

Metallic nanoparticles' antibacterial and anti-inflammatory properties are only a few of the reasons why they are frequently used in biomedical applications. Nano size grants

many advantages to silver-based biomaterials which can be exemplified as addition of a mutation-resistant antimicrobial activity. Most of these nanoparticles are uniquely stable, which means they grow resilience to dissolution and agglomeration.[77]

Silver nanoparticles exhibit an extreme antimicrobial activity in many different routes. Some of the physicochemical properties in these materials are significantly important such as shape, surface charge, concentration, and colloidal state of the nanoparticle. According to these changes, their intrinsic functions like entering a cell or affecting metabolic activities differ. Given a very basic level, their toxicity changes, thus, antibacterial activity directly alters.

Given as a very profitable factor for nano silver-based nanomaterials, they possess unique intrinsic anti-pathogenic effects. Silver cations from these biomaterials are able to bind to thiol groups, due to an affinity of these cations for -S group, of bacterial proteins. When this type of attachment occurs, the physiological actions of bacterial proteins are interfered leading to cell death. Moreover, some DNA lesions might be occurring. Silver-based nanoparticles maintain bacterial activity with Trojan-horse mechanism because first encounter with these particles cause to cell membrane permeability change and cellular respiration depreciation. Inside the cell intracellular metallic silver ion release increases up to extreme levels.[78]

Nanoparticle-assisted treatment may be capable of employing a more comprehensive wound healing. Wound dressing is a therapeutic protective barrier applied directly at the wound. It preserves the wound from external contamination but does not cure it.[79] As a single methodology for both curing and protecting the wound, many functional materials such as hydrogels, hydrofibers, films have been developed. Nanoparticles, as advanced materials in biomedical field, are efficient materials to establish multimodal therapy that can provide synergistic effects.[80] Silver nanoparticles have been efficiently used for antimicrobial applications, thus, wound related infections can easily be treated with proposed quantum dots. NAC has been reported as an antibacterial material. N-acetylcysteine (NAC) is known for its antimicrobial and antibiofilm efficiency that caused 99.9% killing of inoculum. 0,39 mg/ml of NAC was determined as the minimum bactericidal concentration, MBC in a study.[86] NAC has been drawing attention as a powerful antioxidant against pathogens whereas AS-NAC-QD will be experimented together with a photosensitizer, ALA, for the first time on an infected wound region. Within NIR irradiation, ALA has the potential to create ROS or convert light photons to heat. Microorganisms can be destroyed in such a way.[86] NAC integrated nanoparticle

effect on antibacterial and antibiofilm applications would need different evaluation methods. Several factors were used to evaluate nanoparticle effect.

Our group was the first to publish NAC coated Ag_2S QDs with NIR emission. It is proposed here as a new material to provide enhanced antibacterial effects due to NAC coating and mild PTT that may be triggered by Ag_2S irradiation. Photothermal therapy application of these nanoparticles are expected to induce a local temperature increase in the infected wound region to kill the biofilm allowing particle penetration deeper into the biofilm. Photothermal therapy is programmed to be induced at a lower irradiation dose so that healthy tissue would not be affected. Additionally, AS-NAC-QD will be loaded with ALA to induce ALA-PDT over infected wound region in *vivo.* Mild hyperthermia on wound would make bacterial cells in the biofilm more vulnerable to ROS generated by ALA and proceed with ROS-dependent cell death in the prospective region. Hence, ALA loaded AS-NAC-QD can provide a synergistic antibacterial effect via localized temperature increase and ROS generation inhibiting biofilm growth, disrupting the biofilm and killing the bacterial cells, and may be enhancing the healing of the infected area. The focus of this chapter is to divulge in wound-related biofilms and their treatment via combination therapy provided with AS-NAC-QD loaded with ALA.

The hypothesis was tested successfully in vitro by İrem Koç (MS thesis, year 2023, title "Nanoparticle Mediated Diagnosis and Combination Therapy of Bacterial Infections". Here, the idea was tested *in vivo* using Pseudomonas aeruginosa infected burn-wounds. The bacteria tested in this study was Pseudomonas aeruginosa. The rod-shaped bacterium Pseudomonas aeruginosa is commonly found in nature. This aerobic bacterial pathogen is Gram-negative and does not ferment glucose. It is also recognized as an opportunistic pathogen that is resistant to antibiotics and can infect humans and animals with serious infections.[77] In order to minimise bacterial death (false negatives) or contaminant overgrowth (false positives), successful culture needs the collection of representative material.[78] This material should be free of contamination.

Critical steps include NP administration and optimization of laser fluence to bring out an effective therapeutic outcome.

3.2 Materials and Method

3.2.1 Materials

We bought silver nitrate (AgNO3, 99.9999 percent) from Aldrich (MO, USA) and sodium sulfide (Na2S) from Alfa-Aesar in Lancashire, England. N-acetyl-l-cysteine (NAC), acetic acid (CH3COOH), sodium hydroxide (NaOH), sodium chloride (NaCl), 65% Suprapur nitric acid, and 96% Suprapur sulphuric acid were purchased from Merck Millipore (MA, USA). 3 kDa MWCO Vivaspin 20 centrifugal filters were purchased from Goettingen, Germany. Penicillin-streptomycin solutions, trypsin EDTA were purchased from Multicell, Wisent Inc. and 1640 medium (RPMI 1640, 1x). was purchased from Roswell Park Memorial Institute (Canada, Quebec). Fetal bovine serum (FBS) was bought from Capricorn Scientific GmbH, located in Eggendorfergrund, Germany. Phosphate-buffered saline (PBS) tablets and thiazolyl blue tetrazolium bromide (MTT) were purchased from Biomatik Corp. (Canada, ON). 4′,6-diamidino-2-phenylindole (DAPI) and dimethyl sulfoxide Hybri-MaxTM were purchased from Sigma (MO, USA). 4% paraformaldehyde solution in PBS was purchased from Santa Cruz Biotechnology, Inc. (USA, CA).[57] 12-, 24-, and 96-well plates were purchased from Nest Biotechnology Co. Ltd. (China's Wuxi). When water was required, only ultra-pure water (18.2 MΩ, Rephile Biosciences and Technology, Shanghai, China) was used. Every reagent was of the highest purity or analytical grade. Pseudomonas aeruginosa American Type Culture Collection, ATCC, 700829 was used in the experiments in which antimicrobial activity and antibiofilm assay were examined. SPAN 80 was purchased from Sigma Aldrich.

3.2.2 Preparation of nanoparticle integrated crème

Nanoparticle integrated *crème* was synthesized following a facile method. 1 g of gelatin was dissolved in 6 ml of DI water in a vial and set to heat at 80°C. The solution was mixed vigorously until all gelation was dissolved. In another vial, 3 g coconut oil and 2 g SPAN 80, as an emulsifier, were melted and set to heat 80°C. After it was dissolved, 2 vials were added to each other during it was continuously shaken on a heating mantel. 1050 ug/ml Ag amount from AS-NAC-QD was added in 988 ul DI water. Amount of ALA that is relative to Ag amount was taken from 2 mg/ml ALA solution in DI water. Both QD and ALA were added to each other in another vial and then transferred to main reaction mixture. It was taken from the heating mantel when it obtained a viscous

appearance. The solution was shaken at a moderate speed, 300 rpm at room temperature. AS-NAC-QD had NP concentration as 17,8 mg/ml and it contained 10,425 mg/ml Ag concentration.

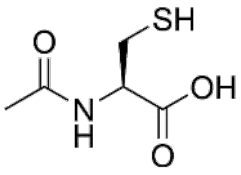

Figure 3.2: Chemical structure of N-acetyl cysteine

3.2.3 Bacteria Culture

For this study, Pseudomonas aeruginosa ATCC® 700829TM was used. Bacteria were streaked on Tryptic Soy Agar, TSA, (NutriSelect® Plus, Sigma). Tryptic Soy Broth (TSB, BDTM BactoTM) was used to inoculate a single colony of bacteria from overnight cultures, which were then incubated for the entire night at 37 °C and 135 rpm. Bacterial suspension was adjusted to McFarland 0.5 (108 CFU/ml) in TSB containing 20% glycerol (Sigma), and bacteria were applied to the wound region at a final concentration of 105 ug/mL. This experiment was conducted by Dr. Nazlı Ataç under the supervision of Prof. Füsun Can at Koç University Hospital.

3.2.4 Biofilm Activity

Biofilms were produced in bacteria media within 96-well plates according to procedure described by Merritt. [52] A single colony was inoculated in TSB for an overnight period at 37 °C [83], and then 0.5 MacFarland cell suspension was seeded into wells with TSB-glucose medium for 24 hours. Subsequently, the media were cautiously extracted from the wells and replaced with solutions of ALA, QDs, or ALA-QDs. Colony counting was used to measure survival of bacteria after a 24-hour incubation period at 37 °C. Following an overnight incubation at 37 °C, biofilms were scraped from the wells and transferred to PCR plates when incubation period was ended. They were homogenised for 5 minutes using microplate sonication (Q Sonica) at 75 Hz. The viability of bacteria was again determined. Colony-forming units, colony forming unit (CFU)/ml levels were compared to the untreated control group. A 2-log (99%) growth reduction as an average CFU/mL value was considered significant. All studies were carried out in triplicates.

The cell suspensions were supplemented with fractional concentrations of 1, 2, and 3 mM ALA; QDs at 262, 352, and 525 ug/ml Ag and ALA-QDs at the same Ag concentrations. These final concentrations were proposed based on the AS-NAC QD study in our lab. [83]

As it will be explained in the next section, application of nanoparticle (containing AS-NAC-QD and ALA) was carried out in three different parts. At Experiment Sets 2 and 3, glycerol-TSB was employed to effectively distribute the bacterial solution across the wound surface. Overnight incubation was used to generate biofilms.

3.2.5 In vivo Application

Based on the *in vitro* applications, the best dosage of 525 ug/ml Ag concentration and 3mM free ALA were used *in vivo* applications. AS-NAC QD and ALA were applied together as the nanoparticle combination on the wound. Application of multimodal therapy was planned in three different sets of experiments. Three sets of experiments consisted of 25 rats, which are to be named as test subjects. In the first set, twelve female Wistar Albino, a *Rattus norvegicus* species, in 4 different groups were enrolled. [84] Each group contained 3 test subjects in the same cage. Koç University Research Center for Translational Medicine (KUTTAM) Animal Research Laboratory took care of the subjects. Test subjects were healthy and 3 months old that weighed 250-300 g. Specific circumstances were provided with 22 °C, light (12/12 hour light/dark cycle), feeding (standard rat food and tap water), and housing (classic plastic confine on sawdust bedding) were all regulated and homogeneous.

3.2.6 Photothermal Therapy

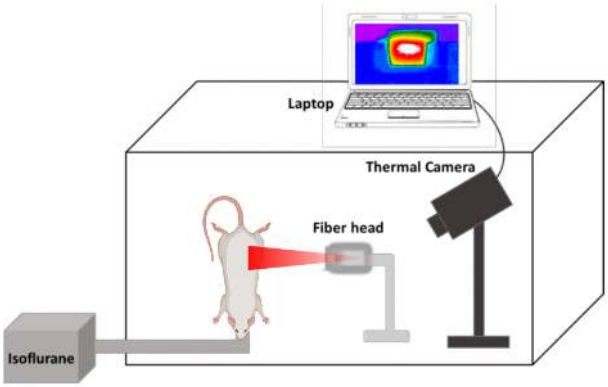

Figure 3.3: Sketch of experimental set up used for *in vivo* experiments performed on rats to see photothermal effect of AS-NAC QDs

Subjects were made put in a position to inhale isoflurane in gas form and continuously breathed that during the application. Rats were shaved and a 1.0 x 1.0 cm hot metal plate was used to create a stripe on the rats' backs in Experiment Set 1. A third-degree burn was created in a few seconds. The strain of Pseudomonas aeruginosa ATCC 700829 was introduced with a patch and wound area was encircled with a line of bandage. After 24-hour incubation of bacteria on the wound, NP solution containing a final concentration of 525 ug/ml was applied to the wound's surface. NP solution included 525 ug/ml Ag and 3 mM ALA. Aqueous nanoparticles were not efficient enough to be fused in a 3rd degree of burn at adipose tissue. Therefore, bacteria solution was transferred into a patch and then applied to the wound. Next day, previous patch was removed, NP was transferred to another patch and applied on the wound again. Experiment Set 1 and different parameters of this set were summarized in Table 3.1.

$$\text{Fluence } \left[\frac{\text{Joules}}{\text{cm}^2}\right] = \frac{\text{Laser pulse energy [J]}}{\text{Effective focal spot area [cm}^2\text{]}}$$

Figure 3.4: Fluence formula of continuous wave laser

Experiment Set 1					
Experiment Set-up			Laser Irradiation Applied		NP added
In separate cages	Experiment Groups	Number of Replicas (Rats) Used	Time (s)	Laser Fluence (J/cm-2)	Concentration (ug/ml)
No	Control	3	0	0	0
No	Wound + NP	3	0	0	525
No	Wound + NP + Min. Fluence (Laser 1 + NP)	3	525	116	525
No	Wound + NP + Max. Fluence (Laser 2 + NP)	3	1050	232	525

Table 3.1: Experiment set-up, Laser application and Nanoparticle addition for Experiment Set 1

640 nm laser was applied to the wound surfaces at a two different fluences. Four different groups of animals were chosen as experiment groups: nanoparticle (NP), control, and laser irradiated nanoparticle applied group (Laser + NP). Laser 1 has the highest fluence of 232 J/cm^{-2} while Laser 2 has the fluence of 116 J/cm^{-2}. Laser fluence was calculated and altered based on the formula in Figure 3.3. On the third day after the burn, the healing of the wound was assessed, and no discernible progress was found. Then, second round of laser application was considered. From the histological results, it seemed hazardous to healthy muscle cells which is discussed later in this chapter. Day 12 of the experiment marked the sacrifice day for the test subjects. Wound surfaces were dissected and sectioned for four groups: histological analysis, bacterial colony count, SEM imaging, and ICP for metal ion detection from the NP. Tissue sections were disintegrated using an IKA T10 homogenizer and the number of bacteria in the wound section was counted successively. Based on following dilutions, bacteria count was calculated using milligram tissue weight. There was no distinguishable variation between the weights of the test subjects. All subjects were daily supervised while their patches and bandages were changed each day.

According to the results obtained from the first set, procedure especially in the application of nanoparticle was changed. AS-NAC-QD together with ALA was applied on the wound as crème.

**The nanoparticle was applied as freshly prepared crème.*					
***Bacterial solution was given with glycerol-TSB.*					
Experiment Set 2					
Experiment Set-up			Laser Irradiation Applied		NP added
In separate cages	Experiment Groups	Number of Replicas (Rats) Used	Time (s)	Laser Fluence (J/cm-2)	Concentration (ug/ml)
Yes	Control	2	0	0	0
Yes	Wound + NP	2	0	0	1050
Yes	Wound + NP + Laser Fluence	2	127	60,06	1050

Table 3.2: Experiment set-up, Laser application and Nanoparticle addition for Experiment Set 2

Nanoparticle integrated crème was produced fresh on application day and spread with an inoculation loop. Also, the bacteria solution was dissolved and transferred on the wound in glycerol. Second change was operated after a mouth bacterium was found in bacterial colony count. This meant that rats tried to nibble each other. They occasionally accomplished corroding one other's bandages and patches. Such was evident and noted down for further experiment sets. That being analysed, each rat was housed individually following daily supervision. A circular metal plate with a diameter of 0.8 cm was used instead of a 1.0 x 1.0 cm metal plate. Its area was exactly same with spot size of the NIR laser used in the animal lab. Considering a problem with the laser power in the first round of studies, we attempted to escalate the power by reducing the spot size, increasing fluence per area.

The fluence was 60,06 J/cm^{-2} for Experiment Set 2 as shown in Table 3.2. 640 nm diode laser with a power arranged to 300 mW was used in Experiment Set 2. Compared to fluences utilised in the first set of experiment, there was no expectation of deep harm or malfunctioning in the tissue.

The nanoparticle was applied as freshly prepared crème.					
**Bacterial solution was given with glycerol-TSB.*					
Experiment Set 3					
Experiment Set-up			Laser Irradiation Applied		NP added
In separate cages	Experiment Groups	Number of Replicas (Rats) Used	Time (s)	Laser Fluence (J/cm-2)	Concentration (ug/ml)
Yes	Control	2	0	0	0
Yes	Wound + NP	2	0	0	1050
Yes	Wound + NP + Min. Fluence	2	600	233	1050
Yes	Wound + NP + Max. Fluence	1	1200	466	1050

Table 3.3: Experiment set-up, Laser application and Nanoparticle addition for Experiment Set 3

In the third set, only laser fluence was altered not to be harmful to animal adipose tissue as it was shown in Table 3.3. It was quite challenging as adipose tissue and normal animal tissue were supposed to have different transmittance. In Set 3, fluence of 233 J/cm^{-2} was applied onto the wound but in a longer duration. Laser was applied for 10 minutes with a spot size of 0,35 cm with 150 mW. Fluence was changed via decreasing the power but increasing the duration. A circular metal plate with a diameter of 0.8 cm was again preferred in Experiment Set 3.

3.3 Results and Discussion

3.3.1 Effect of mild PTT on wound-related biofilms

AS-NAC-QD and ALA loaded AS-NAC-QD were tested for the first time on an bacteria infected wound region. QD effect on burn wounds was demonstrated in several parameters including body weight, wound image, histology results, scanning electron microscopy images and bacterial colony count. Experiment Set 1 was mostly a trial and opened a room for improvement.

Shown in Figure.3.4, body weights of all three experiment sets were recorded and there was no significant difference between test subjects. Wistar albino rats were not

prone to body weight changes, therefore, it was expected for them not to have dramatic changes in body weight.

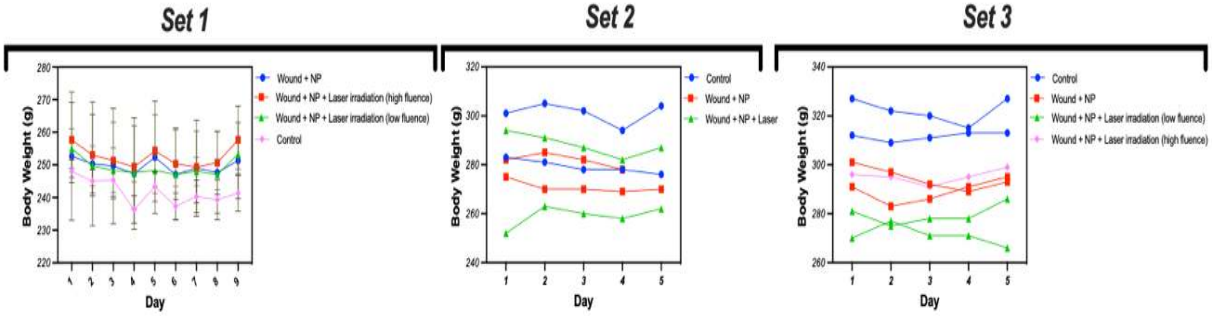

Figure 3.5: Body weights of test subjects (rats) in three different experiment sets

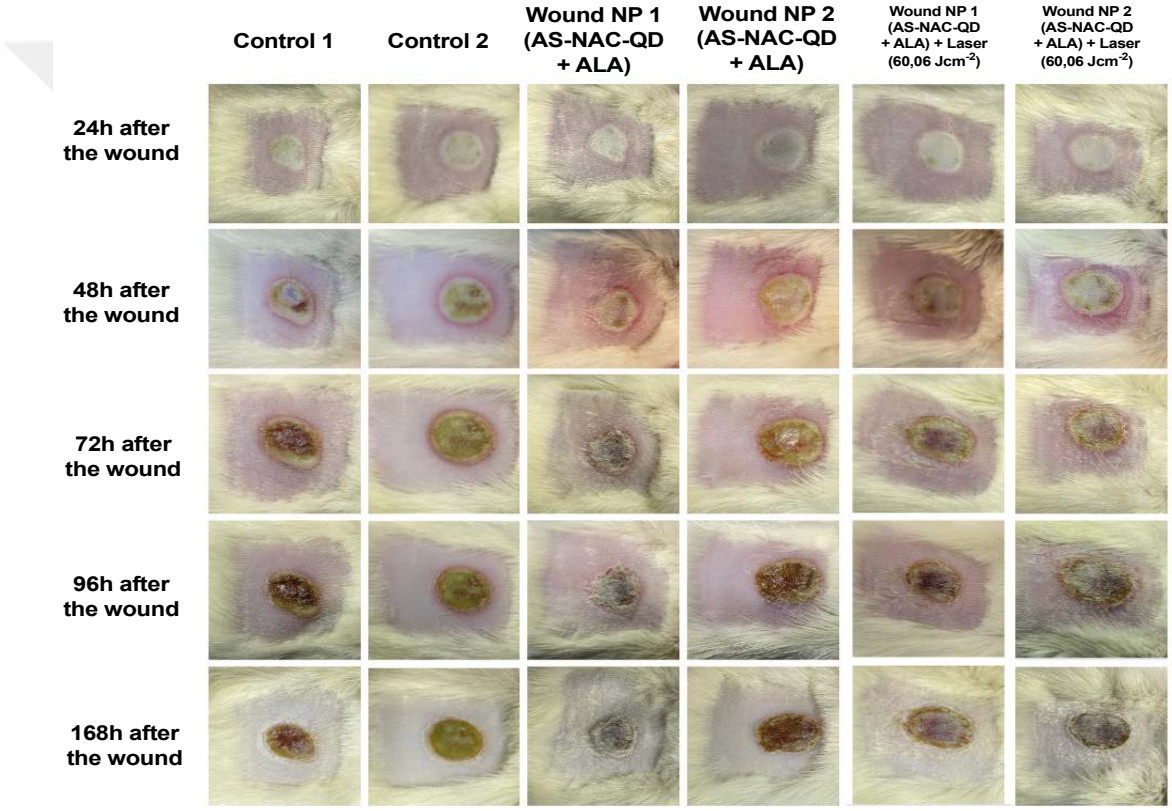

Figure 3.6: Wound images of Experiment Set 2

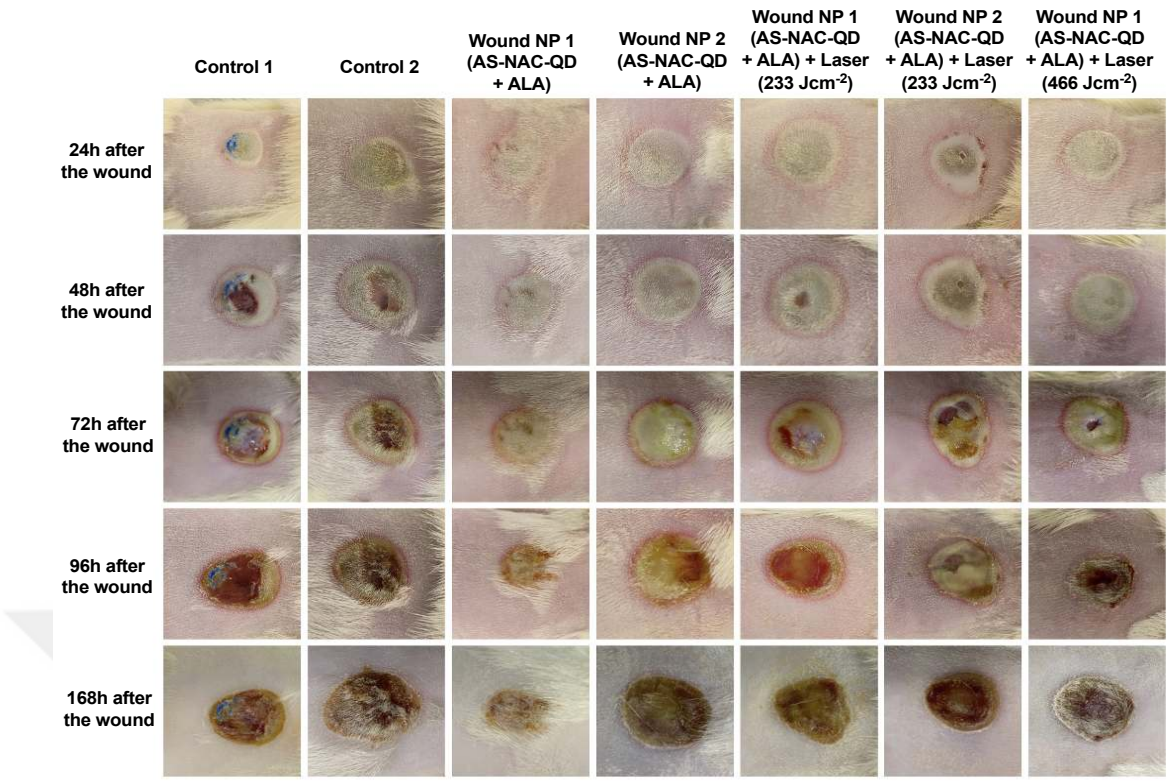

Figure 3.7: Wound images of Experiment Set 3

In Figure 3.5. there is an evident difference between NP treated burn wound and untreated wound. Greenish wound refers to an infected and not healed wound. Even after 168 hours after the burn, tissue did not refresh itself in the control group. After 168 hours passed after the burn, Wound + NP 1 and Wound + NP + Laser 2 groups showed evident healing as it had bristle growing on wound in Figure 3.5. After healing the burn wound infection with a scab, tissue started to back to normal with hair growth induced. These two groups were expected better treatment due to nanoparticle and laser irradiation.

In Figure 3.6., 168 hours after the wound resembled better healing results for Wound + NP 1 and Wound + NP + Laser 3 groups. Bristle grows on the wound referred to an almost complete healing. As shown in Figure 3.6., Control 1 had a thin watery drainage coming from the wound meaning that there was still an untreated infection. Generally, healing starts 48 hours after the burn and continues to enhance via nanoparticle application.

3.3.2 Histology Results

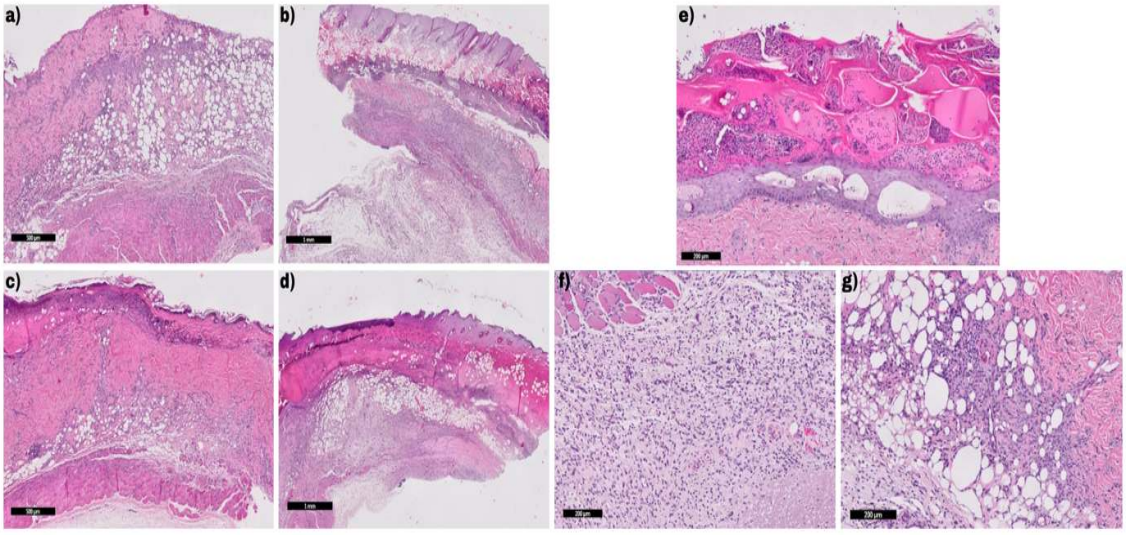

Figure 3.8: Histology examinations of Experiment Set 1 (a-d) and Experiment Set 2 (e-g)

Light microscopy proposes a 0.2 um depth profile of wound tissue. Cells stained with aeosin dye can be analysed to seek healing effect of PTT. Histology and pathology examinations of the wound tissue are shown in Figure 3.7. a) is the untreated control group that had a clear infection, also called as abscess on the upper side of the wound crust. At intermediate phase in reticular layer, established as a spongy layer in between, there is an inflammation. Granulation right next to dermis layer started deep in tissue. Granulation occurs during proliferative phase of wound healing and is apparent seen in Wound + NP group in Figure 3.7. f). Darker colour on wound crust especially in Figure 3.7. d), meaning that Wound + NP + Laser 1 (233 J/cm^{-2}) group, resembles an acute-phase response (APR) inflammation with a higher dose of inflammation. Laser concentrated on a wound surface was extremely high as it can be demonstrated in this sample. There was a necrosis surface on wound crust and even a degenerated collagen layer next to muscle layered in dermis. Second round of high fluence laser probably caused a necrosis surface and induced muscle degeneration in longitudinal axis.

Comparatively, Wound + NP + Laser 2 (116 J/cm^{-2}) group has muscle tissue in contact as it can be seen in lower side of c) in Figure 3.7. Efficient and evident granulation was visible in f) resembling Wound + NP from Experiment Set 2. As it gave the best result in means of wound tissue healing and bacteria growth reduction, it was also noticeable in histology results. Control group was the least effected group meaning that

untreated biofilm caused higher dose of inflammation as it was acknowledged through darker coloured crust of the wound.

3.3.3 Bacterial Colony Count

Bacterial colony count is measured via single colony that is visible to the naked eye, and declared as CFU, colony-forming unit. Different growth measurements will be detected by varying CFU/g values. If there is a 2-log (99%) growth reduction, there will be a significance. Also, bacterial colony count should be matching with histology examinations.

Colony count method following ten-fold serial dilutions was performed in order to detect bacteria growth and its reduction. In Figure 3.8. a) CFU values detected from bacteria growth reduction in Experiment Set 1 were shown. In accordance with data shown, there was no noticeable difference between experiment groups. Wound + NP + Laser 2 (116 J/cm^{-2}), the group that was exposed to minimum laser fluence had the most effective result as it was also supported with histology results. Laser 2 (116 J/cm^{-2}) group induced a healing process and it can be said that it acted as a wound dressing with adequate amount of nanoparticle.

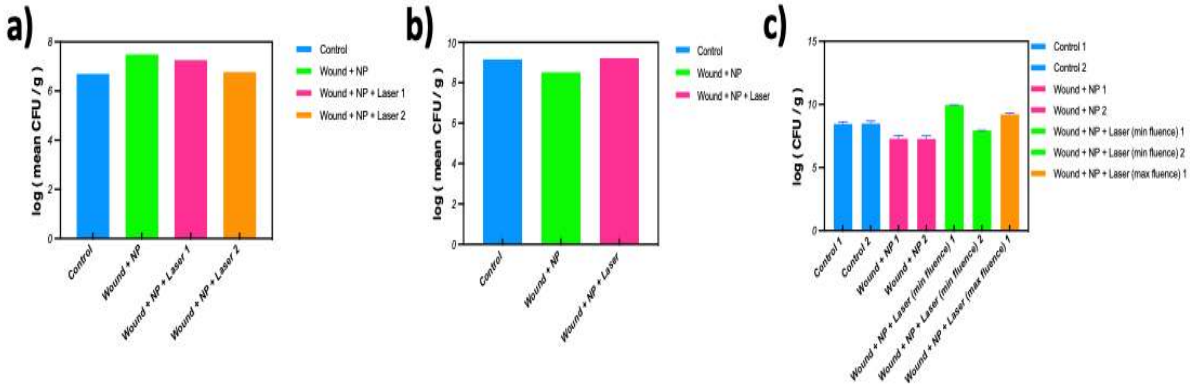

Figure 3.9: Bacteria growth in Experiment Set 1 (a), Experiment Set 2 (b), Experiment Set 3 (c)

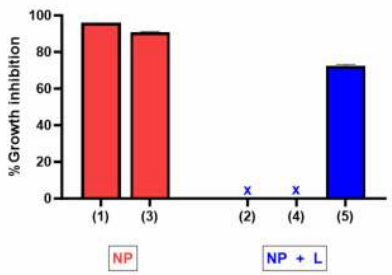

Figure 3.10: Growth inhibition of different groups from Set 3

Second round of experiment had a different result unlike the expected. There was almost a log 2 reduction in Wound + NP group. This established a meaningful result in favour of nanoparticle presence and its application procedure. Laser was applied only in one of the groups as a trial and it did not succeed thermal hyperthermia enough to be shown in bacteria growth reduction in mean CFU. Possible source of error would be inefficiency of photons transferred onto the wound coverage. As a result, a third set with a fresh configuration was operated. There was a growth inhibition in Wound + NP group and also in Wound + NP + Laser application group. It was also visible SEM images below. As explained before, laser fluence was changed via decreasing the power applied and increasing the duration. Probably there was not enough photons coming from the laser irradiation source for PTT. This time, it worked on nanoparticle application as there is a 99% of growth inhibition, so log 2 reduction. Moreover, there is a 72,3% of growth inhibition on the laser applied sample as it is shown in Figure 3.8. c).The number of colonies can also be supported by the density of the bacterial population seen in electron microscopy scanning, SEM, images shown in Figure 3.8. Control groups represent an image composed of whole, not damaged bacteria. Integrity of the bacterial population indicates no healing. Unlike the control group, Wound + NP + Laser treatment groups display incomplete and highly corrupted biofilm appearance. This points out that PTT damaged the biofilm and caused bacterial colony count to drop. SEM images for Experiment Set 1 and 2 were not processed since detection of the burn related wound tissue was not possible.

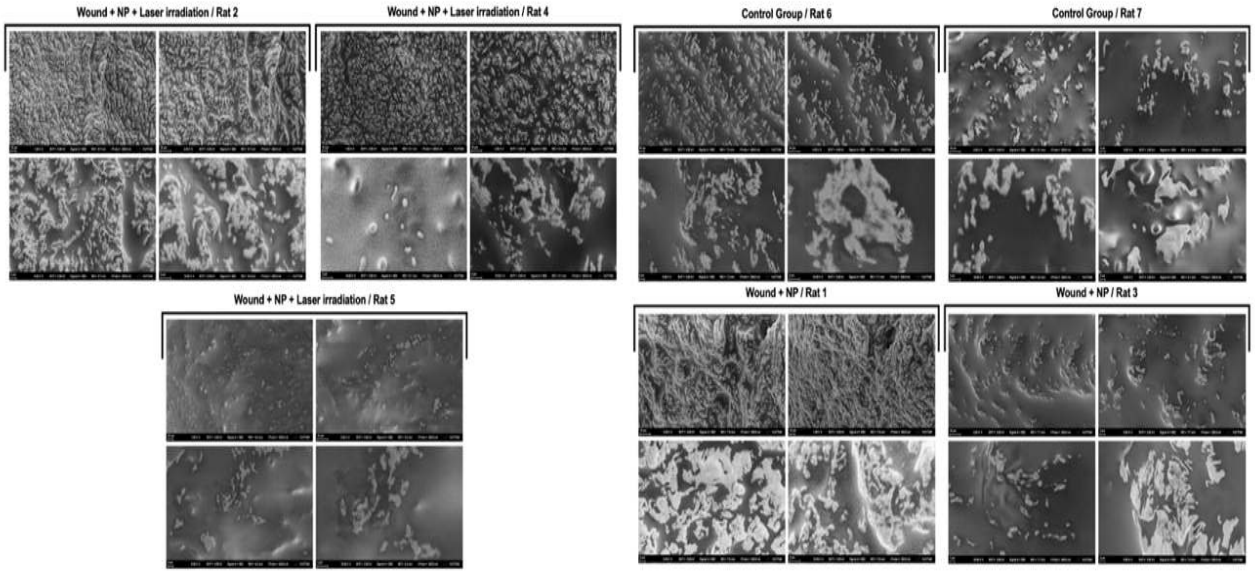

Figure 3.11: SEM images of Set 3

3.3.4 Application of Photothermal Therapy on Wounds

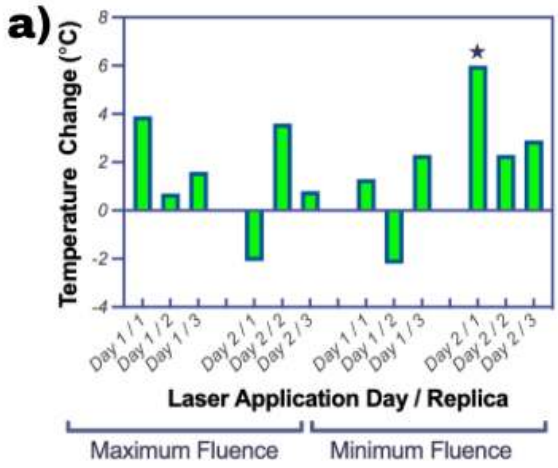

Figure 3.12: Temperature Change from the Experiment Set 1

PTT on eradication of biofilm on wound was applied with 640 nm diode laser, 300 mW, 116 J/cm^{-2} and 232 J/cm^{-2} fluences. Spot size of the laser and wound area created with the 0,8 cm diameter metal plate were not the same in Experiment Set 1. So that, it was adjusted to be exactly same by reducing the burn wound area on the test subjects. PTT was explored via different parameters and matched with the synergistic effect of AS-NAC-QD and ALA on wound. PTT was confirmed with thermal camera images. Matching with the results from histology, bacterial count and images of the wound, Wound + NP + Laser 2 with a (116 J/cm^{-2}) fluence revealed an efficacy of PTT. Mild hyperthermia was concluded with a 6 °C temperature increase as shown in Figure 3.10. With an average, some of other groups also established a mild PTT, however, was not parallel with other results.

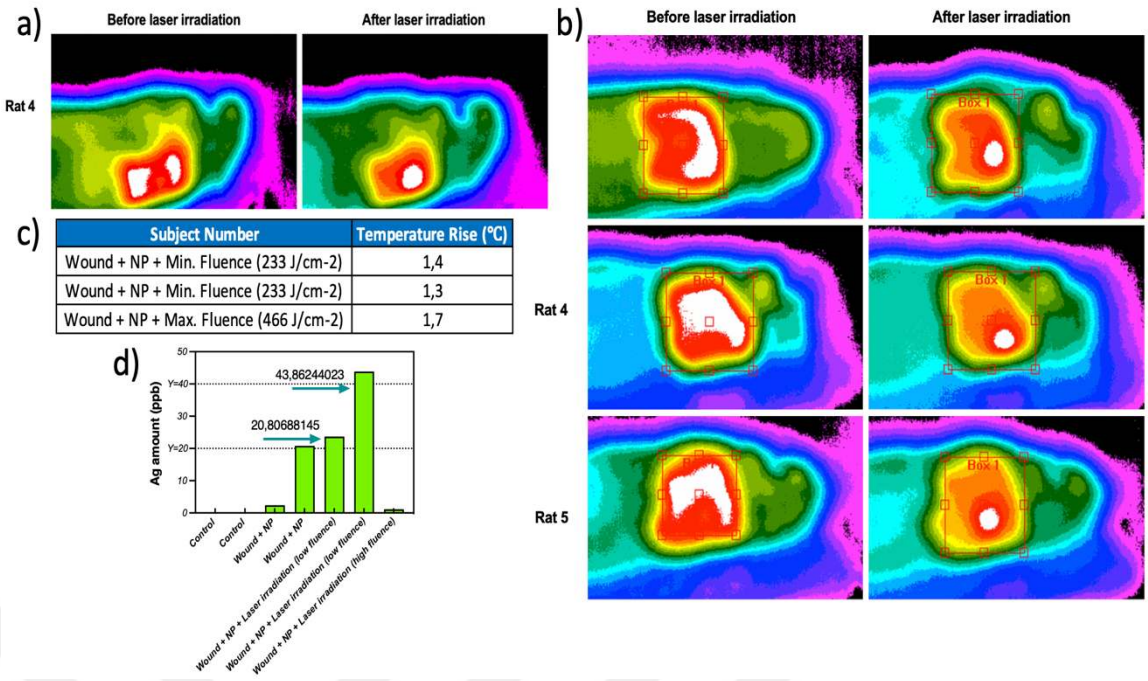

Subject Number	Temperature Rise (°C)
Wound + NP + Min. Fluence (233 J/cm-2)	1,4
Wound + NP + Min. Fluence (233 J/cm-2)	1,3
Wound + NP + Max. Fluence (466 J/cm-2)	1,7

Figure 3.13: Thermal camera images of Experiment Set 2 (a) and Experiment Set 3 (b), Temperature rise of Experiment Set 3 (c), Ag uptake by the biofilm in Experiment Set 3

PTT application was carried out with FLIR thermal camera images as shown in Figure.3.11. Mean temperature rise can be detected via these images for each wound. Temperature increase was calculated as 1.35 °C for samples treated with minimum fluence (233 J/cm^{-2}) in Set 3. These were Rat 2 and Rat 4 as shown in the Figure.3.11 above. This raise was optimised and sufficient for PTT application when it was aligned with Ag uptake by the tissue in Figure 3.11. The highest concentration of Ag, 43 8624 ppb, was taken by Rat 4 and was the best result out of laser irradiation applied group in inhibiting bacterial growth as shown in Figure 3.8. As mentioned in the section 3.2.6., after the day of ex of the test subjects, 1 piece of the burn wound tissue was homogenized and taken for ICP analysis. Uptake of Ag amount was measured via ICP.

3.4 Conclusion

Combined therapy of aPTT and PDT was designed in this study. The combined therapy was designed to eradicate burn-related wound infections. 40 ppb Ag uptake by the tissue resulted in 72.3% bacteria growth reduction. It was a successful result concerning such Ag amount was transferred, however, it could not be repeated. With a higher number of test subjects, laser irradiation with an optimum laser fluence of 233 J/cm^{-2} and NP application as a crème would give more meaningful results. It would be easier to comment whether laser irradiation showed a mean CFU decrease or not. Additionally, 40 ppb Ag uptake may not be optimized so that histological results of Experiment Set 3 should be analysed as well. The results were not readily prepared that is why they could not be included in this thesis.

It showed that AS-NAC-QD should be applied on an adipose tissue with 3rd degree burn as a crème. Otherwise, it cannot interact with the burn wound efficiently as it cannot even dissolve in an environment decorated with 3rd degree burn. Experiment Set 3 showed that only NP transferred to the wound was more efficient when CFU was considered as shown in Figure 3.8. The results demonstrated that AS-NAC-QD was not only a wound dressing but could be potential probes for healing of burn related wounds and infections.

Studied in three separate sets, *in vivo* experiments were conducted, the last of which was successful. Particularly in Experiment Set 3, SEM pictures and CFU values were in accordance. SEM indicated a high rate of corruption in the biofilm whereas bacteria growth inhibition showed over a 70% bacteria growth inhibition. Images of burn-related wounds have additionally contributed to a qualitative understanding of treatment.

3.5 Acknowledgement

This study was funded by TUBITAK (grand number 220S035; PI: Assist. Professor Kübra Onbaşlı and Prof. Havva Yağcı Acar). Bacterial and biofilm related studies were done by Dr. Nazlı Ataç in guidance of Prof. Füsun Can (School of Medicine, Koç University Hospital and Koç University-İşbank Center for Infectious Diseases, KUISCID). Animal experiments were run by DVM. Nilhan Coşkun (KUTTAM Laboratory Animals Research Facility) in my supervision and assistance.

Chapter 4:Perspectives for Future Studies

In this thesis, we designed a portfolio of hybrid nanoparticles and studied their characteristics as well as their structures. Functionalised coatings and up-to-demand feasibilities allow these particles to be eligible for varying usage. Depending on utilisation and purpose, many different functions can be improved on these nanoparticles. Stabilization of this portfolio widened a room for optimisation in several applications, especially in PTT. It would be remarkable to study cancer treatment of these nanoparticles and cell death mechanisms. Especially Hybrid Type 5 can be a promising candidate to work with in vitro and *in vivo* studies. ALA or any other drug can be electrostatically loaded on to seek further therapeutic effects. Further, it would be significant to seek catalytic and electrochemistry activities of these nanoparticles.

Also, *in vivo* studies of antibacterial experiments of AS-NAC-QD would be enhanced with varying doses and laser fluence especially after these optimisation processes. As suggested also in the project proposal, photodynamic therapy induced by ALA *in vivo* studies would be a further improvement. Analysis on ALA working principle via laser irradiation of most promising fluence would be studied. These findings may be fruitful to explore nanoparticle effect in the clinic and lower NAC dosage used as an antibacterial material. Employing confocal microscopy, ROS presence and the PDT effect from ALA can be examined. It would enhance antibacterial properties of AS-NAC-QDs and PTT results. Increasing replicas in this experimental set-up would also reduce standard deviation and indicate a more reliable outcome.

Bibliography

[1] ‘Smart Nanomaterials for Biomedical Applications-A Review’, doi: 10.3390/nano11020396.

[2] ‘Material Nanoarchitectonics of Functional Polymers and Inorganic Nanomaterials for Smart Supercapacitors’, doi: 10.1002/smll.202102397.

[3] ‘designing with smart materials’. [Online]. Available: https://www.outofframe.mit.edu/allposts/designing-with-smart-materials

[4] S. Bocquet, R. J. Pollard, and J. D. Cashion, ‘Dynamic magnetic phenomena in fine-particle goethite’, *Phys. Rev. B*, vol. 46, no. 18, pp. 11657–11664, Nov. 1992, doi: 10.1103/PhysRevB.46.11657.

[5] N. A. Liedienov *et al.*, ‘Critical phenomena of magnetization, magnetocaloric effect, and superparamagnetism in nanoparticles of non-stoichiometric manganite’, *J. Alloys Compd.*, vol. 836, p. 155440, Sep. 2020, doi: 10.1016/j.jallcom.2020.155440.

[6] M. Carbucicchio, C. Grazzi, M. Rateo, G. Ruggiero, M. Solzi, and G. Turilli, ‘Size-dependent magnetic properties in Fe/Al multilayers’, *J. Magn. Magn. Mater.*, vol. 215–216, pp. 563–565, Jun. 2000, doi: 10.1016/S0304-8853(00)00222-5.

[7] ‘The Incredible History of Iron and Steel’, Wisconsin Metal Tech. [Online]. Available: https://wisconsinmetaltech.com/the-incredible-history-of-iron-and-steel/

[8] A. D. Sheftel, A. B. Mason, and P. Ponka, ‘The long history of iron in the Universe and in health and disease’, *Biochim. Biophys. Acta*, 1820.

[9] E. Voloshina, ‘Hematite, Its Stable Surface Terminations and Their Reactivity Toward Water’, doi: https://doi.org/10.1016/B978-0-12-409547-2.14157-5.

[10] ‘Iron Oxide’, Golchha Oxides. [Online]. Available: http://www.golchhaoxides.com/iron-oxide-pigments.php#:~:text=The%20History%20Of%20Iron%20Oxide,drawings%20to%20ensure%20bountiful%20hunting

[11] M. Bloemen *et al.*, ‘Multifunctional iron oxide nanoparticles for biomedical applications’, presented at the SPIE BiOS, W. J. Parak, M. Osinski, and X.-J. Liang, Eds., San Francisco, California, United States, Mar. 2015, p. 933816. doi: 10.1117/12.2076120.

[12] N. Elahi and M. Rizwan, ‘Progress and prospects of magnetic iron oxide nanoparticles in biomedical applications: A review’, *Artif. Organs*, vol. 45, no. 11, pp. 1272–1299, Nov. 2021, doi: 10.1111/aor.14027.

[13] ‘Magnetic nanoparticles and biosciences’, doi: 10.1007/s007060200047.

[14] ‘Superparamagnetism’, Magnetic iron oxide nanoparticles for MR contrast agents. [Online]. Available: https://bme240.eng.uci.edu/students/08s/ykim30/02_1.htm

[15] Wahajuddin and Arora, ‘Superparamagnetic iron oxide nanoparticles: magnetic nanoplatforms as drug carriers’, *Int. J. Nanomedicine*, p. 3445, Jul. 2012, doi: 10.2147/IJN.S30320.

[16] O. Petracic, ‘Superparamagnetic nanoparticle ensembles’, *Superlattices Microstruct.*, vol. 47, no. 5, pp. 569–578, May 2010, doi: 10.1016/j.spmi.2010.01.009.

[17] P. E. Jönsson, ‘Superparamagnetism and Spin Glass Dynamics of Interacting Magnetic Nanoparticle Systems’, in *Advances in Chemical Physics*, 1st ed., vol. 128, S. A. Rice, Ed., Wiley, 2003, pp. 191–248. doi: 10.1002/0471484237.ch3.

[18] G. Nabiyouni, A. Shabani, S. Karimzadeh, J. Ghasemi, and H. Ramazani, ‘Synthesis, characterization and magnetic investigations of Fe3O4 nanoparticles and zeolite-Y nanocomposites prepared by precipitation method’, *J. Mater. Sci. Mater. Electron.*, vol. 26, no. 8, pp. 5677–5685, Aug. 2015, doi: 10.1007/s10854-015-3118-9.

[19] A. J. Szalai, N. Manivannan, and G. Kaptay, ‘Super-paramagnetic magnetite nanoparticles obtained by different synthesis and separation methods stabilized by biocompatible coatings’, *Colloids Surf. Physicochem. Eng. Asp.*, vol. 568, pp. 113–122, May 2019, doi: 10.1016/j.colsurfa.2019.02.006.

[20] A. M. Sanati, S. Kamari, and F. Ghorbani, ‘Application of response surface methodology for optimization of cadmium adsorption from aqueous solutions by Fe3O4@SiO2@APTMS core–shell magnetic nanohybrid’, *Surf. Interfaces*, vol. 17, p. 100374, Dec. 2019, doi: 10.1016/j.surfin.2019.100374.

[21] Y. Portilla *et al.*, ‘Different coatings on magnetic nanoparticles dictate their degradation kinetics *in vivo* for 15 months after intravenous administration in mice’, *J. Nanobiotechnology*, vol. 20, no. 1, p. 543, Dec. 2022, doi: 10.1186/s12951-022-01747-5.

[22] J. Jiang, G. Oberdörster, and P. Biswas, ‘Characterization of size, surface charge, and agglomeration state of nanoparticle dispersions for toxicological studies’, *J.*

Nanoparticle Res., vol. 11, no. 1, pp. 77–89, Jan. 2009, doi: 10.1007/s11051-008-9446-4.

[23] *Applications of Nanocomposite Materials in Drug Delivery*. Elsevier, 2018. doi: 10.1016/C2016-0-05075-1.

[24] R. Kas, E. Sevinc, U. Topal, and H. Y. Acar, 'A Universal Method for the Preparation of Magnetic and Luminescent Hybrid Nanoparticles', *J. Phys. Chem. C*, vol. 114, no. 17, pp. 7758–7766, May 2010, doi: 10.1021/jp100312e.

[25] Z.-Z. Liu, Q. Wang, X. Liu, and J.-Q. Bao, 'Effects of amino-terminated self-assembled monolayers on nucleation and growth of chemical vapor-deposited copper films', *Thin Solid Films*, vol. 517, no. 2, pp. 635–640, Nov. 2008, doi: 10.1016/j.tsf.2008.07.030.

[26] K. Bilici, A. Muti, A. Sennaroğlu, and H. Yagci Acar, 'Indocyanine green loaded APTMS coated SPIONs for dual phototherapy of cancer', *J. Photochem. Photobiol. B*, vol. 201, p. 111648, Dec. 2019, doi: 10.1016/j.jphotobiol.2019.111648.

[27] K. Bilici *et al.*, 'Broad spectrum antibacterial photodynamic and photothermal therapy achieved with indocyanine green loaded SPIONs under near infrared irradiation', *Biomater. Sci.*, vol. 8, no. 16, pp. 4616–4625, 2020, doi: 10.1039/D0BM00821D.

[28] S. Yoffe, T. Leshuk, P. Everett, and F. Gu, 'Superparamagnetic Iron Oxide Nanoparticles (SPIONs): Synthesis and Surface Modification Techniques for use with MRI and Other Biomedical Applications'.

[29] M. Mahmoudi, S. Sant, B. Wang, S. Laurent, and T. Sen, 'Superparamagnetic iron oxide nanoparticles (SPIONs): Development, surface modification and applications in chemotherapy', *Adv. Drug Deliv. Rev.*, vol. 63, no. 1–2, pp. 24–46, Jan. 2011, doi: 10.1016/j.addr.2010.05.006.

[30] J. Y. Ying, Y. Zheng, and S. T. Selvan, 'Synthesis and applications of quantum dots and magnetic quantum dots', presented at the Biomedical Optics (BiOS) 2008, M. Osinski, T. M. Jovin, and K. Yamamoto, Eds., San Jose, CA, Feb. 2008, p. 686602. doi: 10.1117/12.784053.

[31] M. Hashemkhani, 'Development of Ag-based Quantum Dots for Optical Imaging and Multimodal Therapy of Cancer', Koc University.

[32] A. I. Ekimov, L. Efros, and A. A. Onushchenko, 'QUANTUM SIZE EFFECT IN SEMICONDUCTOR MICROCRYSTALS'.

[33] P. Guyot-Sionnest, 'Colloidal quantum dots', *Comptes Rendus Phys.*, vol. 9, no. 8, pp. 777–787, Oct. 2008, doi: 10.1016/j.crhy.2008.10.006.

[34] 'The Types of Recombination in Semiconductors', Cadence System Analysis. [Online]. Available: https://resources.system-analysis.cadence.com/blog/msa2022-the-types-of-recombination-in-semiconductors

[35] 'Quantum Dots', Libre Texts Engineering. [Online]. Available: https://eng.libretexts.org/Bookshelves/Materials_Science/Supplemental_Modules_(Materials_Science)/Semiconductors/Quantum_Dots

[36] 'Band Gap', PV Education. [Online]. Available: https://www.pveducation.org/pvcdrom/pn-junctions/band-gap

[37] A. I. Ekimov *et al.*, 'Absorption and intensity-dependent photoluminescence measurements on CdSe quantum dots: assignment of the first electronic transitions', *J. Opt. Soc. Am. B*, vol. 10, no. 1, p. 100, Jan. 1993, doi: 10.1364/JOSAB.10.000100.

[38] B. Uprety and H. Abrahamse, 'Semiconductor quantum dots for photodynamic therapy: Recent advances', *Front. Chem.*, vol. 10, p. 946574, Aug. 2022, doi: 10.3389/fchem.2022.946574.

[39] L. Wen, L. Qiu, Y. Wu, X. Hu, and X. Zhang, 'Aptamer-Modified Semiconductor Quantum Dots for Biosensing Applications', *Sensors*, vol. 17, no. 8, p. 1736, Jul. 2017, doi: 10.3390/s17081736.

[40] L. Pauksch *et al.*, 'Biocompatibility of silver nanoparticles and silver ions in primary human mesenchymal stem cells and osteoblasts', *Acta Biomater.*, vol. 10, no. 1, pp. 439–449, Jan. 2014, doi: 10.1016/j.actbio.2013.09.037.

[41] A. Nicolae-Maranciuc, D. Chicea, and L. M. Chicea, 'Ag Nanoparticles for Biomedical Applications—Synthesis and Characterization—A Review', *Int. J. Mol. Sci.*, vol. 23, no. 10, p. 5778, May 2022, doi: 10.3390/ijms23105778.

[42] Y. Zhang *et al.*, 'Ag $_2$ S Quantum Dot: A Bright and Biocompatible Fluorescent Nanoprobe in the Second Near-Infrared Window', *ACS Nano*, vol. 6, no. 5, pp. 3695–3702, May 2012, doi: 10.1021/nn301218z.

[43] S. I. Sadovnikov, A. V. Ishchenko, and I. A. Weinstein, 'Optical properties of Ag_2S quantum dots', *Mater. Sci. Eng. B*, vol. 296, p. 116667, Oct. 2023, doi: 10.1016/j.mseb.2023.116667.

[44] D. Aydemir, M. Hashemkhani, H. Y. Acar, and N. N. Ulusu, 'Evaluation of the biocompatibility of the GSH-coated Ag_2S quantum dots in vitro: a perfect example

for the non-toxic optical probes', *Mol. Biol. Rep.*, vol. 47, no. 6, pp. 4117–4129, Jun. 2020, doi: 10.1007/s11033-020-05522-3.

[45] M. Gao, H. Zhao, Z. Wang, Y. Zhao, X. Zou, and L. Sun, 'Controllable preparation of Ag_2S quantum dots with size-dependent fluorescence and cancer photothermal therapy', *Adv. Powder Technol.*, vol. 32, no. 6, pp. 1972–1982, Jun. 2021, doi: 10.1016/j.apt.2021.04.011.

[46] D. Segets *et al.*, 'Determination of the Quantum Dot Band Gap Dependence on Particle Size from Optical Absorbance and Transmission Electron Microscopy Measurements', *ACS Nano*, vol. 6, no. 10, pp. 9021–9032, Oct. 2012, doi: 10.1021/nn303130d.

[47] M. Hashemkhani, K. Bilici, A. Muti, A. Sennaroglu, and H. Y. Acar, 'Ag $_2$ S-Glutathione quantum dots for NIR image guided photothermal therapy', *New J. Chem.*, vol. 44, no. 14, pp. 5419–5427, 2020, doi: 10.1039/C9NJ04608A.

[48] M. Hashemkhani, M. Loizidou, A. J. MacRobert, and H. Yagci Acar, 'One-Step Aqueous Synthesis of Anionic and Cationic AgInS $_2$ Quantum Dots and Their Utility in Improving the Efficacy of ALA-Based Photodynamic Therapy', *Inorg. Chem.*, vol. 61, no. 6, pp. 2846–2863, Feb. 2022, doi: 10.1021/acs.inorgchem.1c03298.

[49] Rodwell, *Harper's Illustrated Biochemistry 31/e*, 31st edition. New York: McGraw-Hill Medical, 2018.

[50] H. R. A. K. Al-Hetty *et al.*, 'Nanomaterials for combination cancer photothermal therapy', *Emergent Mater.*, vol. 6, no. 2, pp. 425–438, Apr. 2023, doi: 10.1007/s42247-023-00464-5.

[51] T. P. Pivetta, C. E. A. Botteon, P. A. Ribeiro, P. D. Marcato, and M. Raposo, 'Nanoparticle Systems for Cancer Phototherapy: An Overview', 2021.

[52] N. Atac, K. Onbasli, I. Koc, H. Yagci Acar, and F. Can, 'Fimbria targeting superparamagnetic iron oxide nanoparticles enhance the antimicrobial and antibiofilm activity of ciprofloxacin against quinolone-resistant *E. coli*', *Microb. Biotechnol.*, vol. 16, no. 11, pp. 2072–2081, Nov. 2023, doi: 10.1111/1751-7915.14327.

[53] M. Hashemkhani, M. Loizidou, A. J. MacRobert, and H. Yagci Acar, 'One-Step Aqueous Synthesis of Anionic and Cationic AgInS $_2$ Quantum Dots and Their Utility in Improving the Efficacy of ALA-Based Photodynamic Therapy', *Inorg. Chem.*, vol. 61, no. 6, pp. 2846–2863, Feb. 2022, doi: 10.1021/acs.inorgchem.1c03298.

[54] P. T. Buz *et al.*, 'Development of near-infrared region luminescent N-acetyl-L-cysteine-coated Ag 2 S quantum dots with differential therapeutic effect', *Nanomed.*, vol. 14, no. 8, pp. 969–987, Apr. 2019, doi: 10.2217/nnm-2018-0214.

[55] F. Chen and W. Cai, Eds., *Hybrid Nanomaterials: Design, Synthesis, and Biomedical Applications*, 1st ed. CRC Press, 2017. doi: 10.1201/9781315370934.

[56] I. Hocaoglu *et al.*, 'Development of highly luminescent and cytocompatible near-IR-emitting aqueous Ag_2S quantum dots', *J. Mater. Chem.*, vol. 22, no. 29, p. 14674, 2012, doi: 10.1039/c2jm31959d.

[57] P. T. Buz *et al.*, 'Development of near-infrared region luminescent N-acetyl-L-cysteine-coated Ag_2S quantum dots with differential therapeutic effect', *Nanomed.*, vol. 14, no. 8, pp. 969–987, Apr. 2019, doi: 10.2217/nnm-2018-0214.

[58] D. Zhao, Z. He, W. H. Chan, and M. M. F. Choi, 'Synthesis and Characterization of High-Quality Water-Soluble Near-Infrared-Emitting CdTe/CdS Quantum Dots Capped by *N* -Acetyl- L -cysteine Via Hydrothermal Method', *J. Phys. Chem. C*, vol. 113, no. 4, pp. 1293–1300, Jan. 2009, doi: 10.1021/jp808465s.

[59] J. Wang *et al.*, 'One-pot synthesis of highly luminescent *N* -acetyl- L -cysteine-capped CdTe quantum dots and their size effect on the detection of glutathione', *New J. Chem.*, vol. 42, no. 19, pp. 15743–15749, 2018, doi: 10.1039/C8NJ02864H.

[60] M. J. Palimi, M. Rostami, M. Mahdavian, and B. Ramezanzadeh, 'Surface modification of Fe 2 O 3 nanoparticles with 3-aminopropyltrimethoxysilane (APTMS): An attempt to investigate surface treatment on surface chemistry and mechanical properties of polyurethane/Fe 2 O 3 nanocomposites', *Appl. Surf. Sci.*, vol. 320, pp. 60–72, Nov. 2014, doi: 10.1016/j.apsusc.2014.09.026.

[61] A. Venerando *et al.*, 'Biotechnological applications of nanostructured hybrids of polyamine carbon quantum dots and iron oxide nanoparticles', *Amino Acids*, vol. 52, no. 2, pp. 301–311, Feb. 2020, doi: 10.1007/s00726-019-02721-6.

[62] S. Kizilel, C. Nazli, Ergenc, Acar, and Yar, 'RGDS-functionalized polyethylene glycol hydrogel-coated magnetic iron oxide nanoparticles enhance specific intracellular uptake by HeLa cells', *Int. J. Nanomedicine*, p. 1903, Apr. 2012, doi: 10.2147/IJN.S29442.

[63] K. Onbasli *et al.*, 'The improved killing of both androgen-dependent and independent prostate cancer cells by etoposide loaded SPIONs coupled with NIR irradiation', *Biomater. Sci.*, vol. 10, no. 14, pp. 3951–3962, 2022, doi: 10.1039/D2BM00107A.

[64] 'Outstanding Reviewers for Photochemical and Photobiological Sciences in 2017', *Photochem. Photobiol. Sci.*, vol. 17, no. 5, pp. 533–533, May 2018, doi: 10.1039/c8pp90021c.

[65] I. Hocaoglu *et al.*, 'Cyto/hemocompatible magnetic hybrid nanoparticles (Ag_2S–Fe3O4) with luminescence in the near-infrared region as promising theranostic materials', *Colloids Surf. B Biointerfaces*, vol. 133, pp. 198–207, Sep. 2015, doi: 10.1016/j.colsurfb.2015.05.051.

[66] F. Varenne *et al.*, 'Evaluation of zeta potential of nanomaterials by electrophoretic light scattering: Fast field reversal versus Slow field reversal modes', *Talanta*, vol. 205, p. 120062, Dec. 2019, doi: 10.1016/j.talanta.2019.06.062.

[67] M. Muzzio, J. Li, Z. Yin, I. M. Delahunty, J. Xie, and S. Sun, 'Monodisperse nanoparticles for catalysis and nanomedicine', *Nanoscale*, vol. 11, no. 41, pp. 18946–18967, 2019, doi: 10.1039/C9NR06080D.

[68] C. Xu and S. Sun, 'Monodisperse magnetic nanoparticles for biomedical applications', *Polym. Int.*, vol. 56, no. 7, pp. 821–826, Jul. 2007, doi: 10.1002/pi.2251.

[69] L. S. Lunin, S. N. Chebotarev, A. S. Pashchenko, and S. A. Dudnikov, 'Correlation between the size and photoluminescence spectrum of quantum dots in InAs-QD/GaAs', *J. Surf. Investig. X-Ray Synchrotron Neutron Tech.*, vol. 7, no. 1, pp. 36–40, Jan. 2013, doi: 10.1134/S1027451013010138.

[70] Y. Hu *et al.*, 'Preparation and optical properties of magnetic carbon/iron oxide hybrid dots', *RSC Adv.*, vol. 7, no. 65, pp. 41304–41310, 2017, doi: 10.1039/C7RA07220A.

[71] M. R. Kasimova, 'Troubleshooting guide for Isothermal Titration Calorimetry'.

[72] J. Leonard, 'How to recognize and treat an infected wound', Medical News Today. [Online]. Available: https://www.medicalnewstoday.com/articles/325040

[73] K. Abbasi *et al.*, 'The wound healing effect of collagen/adipose-derived stem cells (ADSCs) hydrogel: *In vivo* study'.

[74] A. Kushwaha, L. Goswami, and B. S. Kim, 'Nanomaterial-Based Therapy for Wound Healing', *Nanomaterials*, vol. 12, no. 4, p. 618, Feb. 2022, doi: 10.3390/nano12040618.

[75] K. S. Brandenburg *et al.*, 'Development of *Pseudomonas aeruginosa* Biofilms in Partial-Thickness Burn Wounds Using a Sprague-Dawley Rat Model', *J. Burn Care Res.*, vol. 40, no. 1, pp. 44–57, Jan. 2019, doi: 10.1093/jbcr/iry043.

[76] M. M. Mihai, M. B. Dima, B. Dima, and A. M. Holban, ‘Nanomaterials for Wound Healing and Infection Control’, *Materials*, vol. 12, no. 13, p. 2176, Jul. 2019, doi: 10.3390/ma12132176.

[77] A.-C. Burdușel, O. Gherasim, A. M. Grumezescu, L. Mogoantă, A. Ficai, and E. Andronescu, ‘Biomedical Applications of Silver Nanoparticles: An Up-to-Date Overview’, *Nanomaterials*, vol. 8, no. 9, p. 681, Aug. 2018, doi: 10.3390/nano8090681.

[78] S. Mekić, K. Matanović, and B. Šeol, ‘Antimicrobial susceptibility of *Pseudomonas aeruginosa* isolates from dogs with otitis externa’, *Vet. Rec.*, vol. 169, no. 5, pp. 125–125, Jul. 2011, doi: 10.1136/vr.d2393.

[79] C. Xu, O. U. Akakuru, X. Ma, J. Zheng, J. Zheng, and A. Wu, ‘Nanoparticle-Based Wound Dressing: Recent Progress in the Detection and Therapy of Bacterial Infections’, *Bioconjug. Chem.*, vol. 31, no. 7, pp. 1708–1723, Jul. 2020, doi: 10.1021/acs.bioconjchem.0c00297.

[80] S. Aslam and R. O. Darouiche, ‘Role of Antibiofilm-Antimicrobial Agents in Controlling Device-Related Infections’, *Int. J. Artif. Organs*, vol. 34, no. 9, pp. 752–758, Sep. 2011, doi: 10.5301/ijao.5000024.

[81] F. Allerton and T. Nuttall, ‘Antimicrobial use: importance of bacterial culture and susceptibility testing’, *In Pract.*, vol. 43, no. 9, pp. 500–510, Nov. 2021, doi: 10.1002/inpr.139.

[82] Y.-H. Kang, C.-S. Park, and M.-S. Han, ‘Pseudomonas aeruginosa UCBPP-PA14 a useful bacterium capable of lysing Microcystis aeruginosa cells and degrading microcystins’, *J. Appl. Phycol.*, vol. 24, no. 6, pp. 1517–1525, Dec. 2012, doi: 10.1007/s10811-012-9812-6.

[83] İ. Koç, ‘Nanoparticle Mediated Diagnosis and Combination Therapy of Bacterial Infections’, Koc University, Koc University.

[84] I. Durur-Subasi *et al.*, ‘Does the cardiovascular drug levosimendan prevent iodinated contrast medium nephrotoxicity with glycerol aggravation in rats?’, *Eur. Radiol. Exp.*, vol. 5, no. 1, p. 49, Dec. 2021, doi: 10.1186/s41747-021-00249-7.

[85] J.-H. Moon, Y.-S. Choi, H.-W. Lee, J. S. Heo, S. W. Chang, and J.-Y. Lee, ‘Antibacterial effects of N-acetylcysteine against endodontic pathogens’, *J. Microbiol.*, vol. 54, no. 4, pp. 322–329, Apr. 2016, doi: 10.1007/s12275-016-5534-9.

[86] L. Jiang and S. C. J. Loo, ‘Intelligent Nanoparticle-Based Dressings for Bacterial Wound Infections’, *ACS Appl. Bio Mater.*, vol. 4, no. 5, pp. 3849–3862, May 2021, doi: 10.1021/acsabm.0c01168.